Journal of Computation and Artificial Intelligence in Mechanics and Biomechanics

Journal of Computation and Artificial Intelligence in Mechanics and Biomechanics

Editorial overview by

Editor in chief: Jorge Belinha [1]

[1]*School of Engineering, Polytechnic of Porto (ISEP), Department of Mechanical Engineering, Portugal, job@isep.ipp.pt*

Journal of Computation and Artificial Intelligence in Mechanics and Biomechanics (JCAIMB) is a scholarly online peer review free open access journal fully sponsored by "Publicações ISEP". All manuscripts are available in the ZENODO repository database, from OpenAIRE project, allowing an automatically abstracting and indexation and free open access.

Thus, JCAIMB is committed to ensure free Open Science to both authors and readers and to publish only quality works, which are reviewed by experts in related field. Thus, JCAIMB aims to publish quality original research works, following the scientific method of scholarly value in computational mechanics and biomechanics combined with several degrees of artificial intelligence, whose formulations and applications are properly demonstrated and validated. Nevertheless, innovative applications using commercial software packages are encouraged, as well as original and up-to-date revision manuscripts. In this inaugural number of the Journal of Computation and Artificial Intelligence in Mechanics and Biomechanics

In this inaugural number, four manuscripts are published in JCAIMB:

- Artificial Intelligence in Computational Mechanics and Biomechanics, by Jorge Belinha;
- Using advanced discretization techniques to simulate the suturing process, by Ana Guerra, Jorge Belinha and Renato Natal Jorge;
- Artificial Neural Networks Applied in Mechanical Structural Design, by J.P.A. Ribeiro, L.F.F. Gomes and S.M.O. Tavares;
- Free vibration analysis of erythrocytes using the constant strain finite elements: a 3D study, by M. I. A. Barbosa, J. Belinha and R. Natal Jorge.

Enjoy.

The editorial team.

Artificial Intelligence in Computational Mechanics and Biomechanics

Jorge Belinha [1]

[1]*School of Engineering, Polytechnic of Porto (ISEP), Department of Mechanical Engineering, Portugal, job@isep.ipp.pt*

Abstract

This work aims to deliver a brief presentation and evolution of Artificial intelligence (AI) and its potentially most suited methodologies for Computational Mechanics and Biomechanics (CM&B) applications, such as Machine Learning (ML), Pattern Recognition (PR), Deep Learning (DL) and DL using artificial Neural Networks (NN). Afterwards, since DL using artificial NN is the AI methodology mostly used in CM&B, this methodology applied to CM&B problems is described with more detail. In order to show the evolution of AI methodologies in CM&B, a large document search was performed in the academic database Web of Science. Thus, peer-reviewed relevant articles addressing the topics of ML, PR, DL and NN combined with CMB&B were selected for a quantitative analysis. The results confirm that DL using artificial NN is in fact the most used AI methodology in both CM&B. Furthermore, it was found that research using DL using artificial NN combined with the finite element method is growing much faster than any other methodology combination. This work shows the inevitable growth of AI, which will accelerate the computation of today's demanding problems and will allow the simulation of highly complex problems beyond the competence of existing rigid computational methodologies. AI offers the opportunity to expand the traditional application fields of CM&B, which will change its paradigm in a very near future.

1 Introduction

To this day, Computational Mechanics and Biomechanics (CM&B) were supported by well-established computer science branches, such as: mathematical foundations; algorithms and data structures; computer graphics; concurrent, parallel and distributed systems; programming languages and compilers; scientific computing; software engineering; and theory of computation. However, modern CM&B interest fields started to become much more complex and challenging than traditional research areas, and standard computational techniques became insufficient to answer to such demanding problems. Thus, very recently, computational mechanics has started to interact with another fields of computer science, such as Artificial Intelligence (AI) and analytical databases [1,2].

AI, formally introduced in 1956 by Russell et al. [3], is a vast computer science branch, possessing specific research techniques and terminology depending on the research topic. The core techniques of AI have the potential to radically change the biomechanical and structural modelling and programming as we know it. High-level AI techniques and programming are capable to implement advanced methodologies to develop, enhance and apply new numerical methods that defy human comprehension, allowing to achieve more efficient computational mechanics algorithms/codes and more realistic multiscale material constitutive laws. In order to solve engineering problems, AI attempts to capture the principle of human cognition by means of symbol manipulation and symbolically structured knowledge. However, in contradiction, AI solutions frequently defy traditional and analytical methodologies under human linear comprehension.

Today, AI is widely spread by many science fields and several terms also denoting AI are mentioned in the literature, which can cause confusion [1]. Two very close terms are machine intelligence [4] and cognitive computing [5]. Although sometimes used a synonyms, MI and AI are actually distinct concepts. Machine Intelligence (MI) deals with machines with human-like reasoning and behaviour. On the other hand, AI deals with algorithms attempting to reproduce the human reasoning and intelligent behaviour. AI tries to replicate the human cognitive functions and performing the same tasks faster and more accurately. Cognitive Computing (CC), associated with the competences of the human mind, refers to the in-silico replication of human reasoning. CC is a highly challenging field, focusing in the development of algorithms capable of recognizing patterns, training and learning and interpreting big data. In opposition to AI, which

Corresponding Author:
Jorge Belinha
job@isep.ipp.pt

requires an (internal or external) entity deciding which actions are to be taken during the training process, CC is capable to learn, reason and interact as/with a human [1].

With the increase of the available computational power, the general scientific community started to focus in AI. Engineering is no exception. The partnership between CM&B with AI is still in its infancy. However, even today, it is possible to predict and visualize several challenging and promising research fields combining this exciting computation science branch with innovative CM&B approaches. Although AI possesses several methodologies, this work will focus only in four AI techniques presenting a strong potential in CM&B: Machine Learning (ML), Pattern Recognition (PR), Deep Learning (DL) and DL using artificial Neural Networks (NN). Although DP can include propositional formulas or latent variables architectures, most modern DP models are based on artificial NN architectures. Thus, the NN term is frequently used as a substitute term for DL.

2 Artificial Intelligence

It is possible to classify machine intelligence as hard computing or soft computing techniques [1]. Hard computing is the most used in CB&B, it is based in numerical analysis, binary and Boolean logic. Requiring analytical models and rigid and well-defined formulations, hard computing is capable to deliver accurate, robust and repeatable solutions. In this conventional and deterministic computing, the programming code is written, which always provides the same output field solution for the same input variables. In opposition, by including stochastic formulations, parallelization and handling noisy and ambiguous data, soft computing is capable to autonomously develop further its own algorithms and deliver approximate solutions in a fraction of time. Generally, when compared with hard computing, soft computing is less accurate, however it is much faster. Some authors use the term Computational Intelligence (CI) instead soft computing [6]. In order to provide solutions for highly complex problems, CI combines probabilistic methods, fuzzy logic, evolutionary computing, artificial neural networks and learning theory. Most of the problems in biomechanics and micro-mechanics involve numerous input variables, most of which are stochastically uncertain or unobservable. Such difficulty, associated with the process complexity, hinders the use or the development of accurate/useful mathematical models. By means of sample data or experimental observation, CI allows to develop new nonlinear rules approximating a solution using nature-inspired computational techniques [7]. Although their definitions overlap, today it is establish that CI is one of the many subsets of AI [8]. Another two relevant subsets of AI are data science and data mining. Data science/mining uses data to disclose trends, which can then allow to understand complex phenomena and provide much accurate predictions than incomplete or approximated formulations from hard computing. If the data used in data science/mining is large in volume, frequency and diversity, such data is denoted as "big data". Notice that the volume of the data is related with the number of data points (the observable results), the frequency is associated with the number of data acquired per unit of time and the diversity is related with the distinct types of data acquired (material distribution, volume fraction, species, etc.). Due to the large volume, frequency and diversity of these data sets, the data processing techniques traditionally used in hard computing are not capable to interpret or represent big data. As already mentioned, machine learning is an AI methodology. ML uses training data to learn and develop models which are capable to deliver trends and predictions. Deep learning, as a subset of ML, was developed to analyse big data and identify trends and classify data into categories. Fig.1(a) represents the connection between AI methodologies.
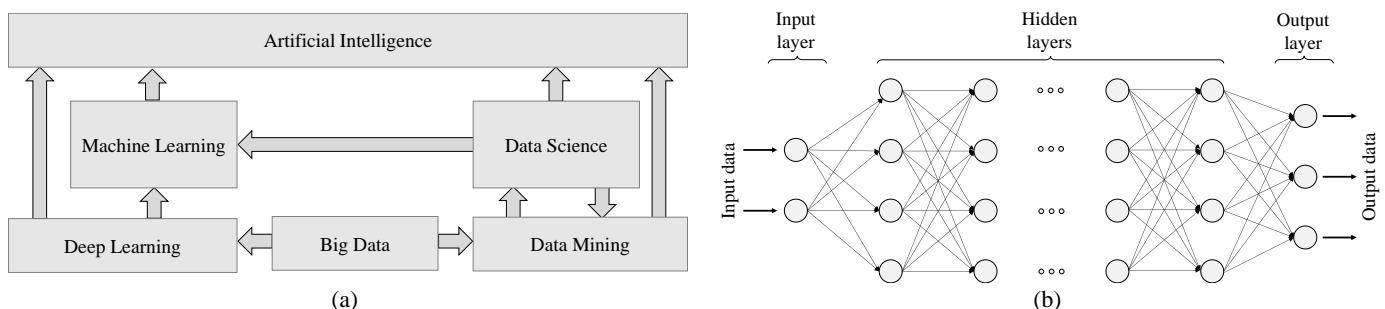

Fig.1 - (a) Schematic representation of the connection between AI methodologies; (b) Feed forward neural network consisting of one input layer, several hidden layers, one output layer. Each layer containing one or more units.

In fact, in CM&B the problem solution strongly depends on decisions, such as the problem domain (scale, size, dimension, geometry, etc.), the boundary conditions (initial imposed variable fields, variable constrains, etc.), the material uncertainties (mechanical properties, heterogeneity, anisotropy, constitutive model, etc.) methodology

(continuous methods, discrete techniques, machine precision, etc.) and the formulation (elastic, hyperelastic, elastoplastic, damage mechanics, fracture mechanics, heat-transfer, fluid mechanics, etc.). These decisions are made by humans, and the solution's accuracy is highly influenced by the experience and knowledge of the researcher/engineer. Most of these decisions could be done by AI techniques, such as selecting the most accurate number of integration points per integration cell in a finite element analysis [2]. Due to the unique character of the problems involved in CM&B, hard computation is still its mainstream process. Past experience can be encoded and turned into big data, which can then be analysed and converted into trends and AI rules. AI methodologies are becoming increasingly useful, as shown by the CM&B applications combined with deep learning and model order reduction [9] or multiscale homogenization techniques [10].

3 Deep learning and Neural Networks in CM&B

The AI, using artificial NN, the core technique of DL, has already been tested and applied in relevant computational mechanics fields [2,11]. Artificial NN can be classified by their architectural structure as "feed forward neural networks" or "mutually connected neural networks". In Fig.1(b) is shown a schematic representation of a feed forward neural network. As shown in the extensive review in [2], since artificial NN are capable of nonlinear mapping, NN are suitable to estimate crack growth [12], enhance contact algorithms [13] and improve the nonlinear solution methods [14] and variational formulations [15], among many other applications.

In fact, for complex problems, artificial NN require long training, demand a high computational cost, and present a low convergence. One possible solution is to simplify the problem. Therefore, until now, the majority of the artificial NN implemented in computational mechanics used simple and reduced amount of learning patterns and epochs. Thus, the simulated mapping of those applications is basic and its solutions space is narrowed. Fortunately, in the last few years, computational power and processor architectures have improved significantly and training algorithms for artificial NN have been enhanced considerably. This combined events allow to train large NN, entering the DL field. Thus, artificial NN with DL have become accessible to study much more complex problems within the CM&B fields.

In standard CM&B, first, it is necessary to identify or develop the partial differential equation ruling the physical or biological phenomena under study. Then, combining it with a discretization technique, the system of equations is established and, after setting the essential and natural boundary conditions, the system of equations is solved numerically. All the steps and rules for solving the process were developed by human and all decisions are human dependent. It was the human observation of physical or biological phenomena, combined with its mathematical comprehension, that allowed to develop the partial differential equations and constitutive material laws available in the literature. All the rules developed by humans are limited by human's natural perception, intellectual capacity and acquired awareness.

AI permits to expand and amplify human's intelligence. For instances, ML using DL and artificial NN allowed to process large amount of random and unstructured data, offering the possibility to discover automatically new rules. Regarding the ability to find and develop new rules, the literature shows that, among ML methods, DL is superior to any other technique [2]. Using large data sets, DL is capable to discover rules that are too much complex to be understood by human's comprehension. DL rules are not explicit rules, mathematical equations or structured algorithms, possessing explicit symbolic representations within human's cognitive bound. DL rules are represented by implicit mapping, being flexible enough to adapt to new training data or human's input. When compared with explicit rules, DL is capable to handle with higher efficiency the complex relation between the several variables and parameters involved in the observed phenomenon. Thus, DL is able to develop the mapping associating those variables and parameters and, at the same time, update and evolve the mapping with new data. In order to implement DL with artificial NN in CM&B, the following phases can be generically followed [2].

Data preparation phase: an input-output association is established, being the input represented by the n-dimensional vector $\Psi = \{\psi_1^p, \psi_2^p, ..., \psi_n^p\}$ and the output represented by the m-dimensional vector $\Phi = \{\phi_1^p, \phi_2^p, ..., \phi_m^p\}$. Each component of vectors Ψ and Φ can be an integer or real number. The superscript p indicates the pth data pairs of a large data set of pair. It is recommended to gather and use a representative number of data pairs in order to efficiently establish the mapping relation between them. Such massive gathering can be achieved using CM&B analyses.

Training phase: in this phase DL starts the training aiming to achieve the mapping rules governing the input-output data pairs gathered in the data preparation phase. Thus, an artificial NN considers the n-dimensional input-data contained in Ψ as the input to the NN and, as corresponding teacher signal, the artificial NN considers the m-dimensional vector $\Phi = \{\phi_1^p, \phi_2^p, ..., \phi_m^p\}$. Errors and deviations are calculated between the input and the output towards convergence.

When convergence is achieved, multi-dimensional mapping is attained: $\mathbb{R}^n \to \mathbb{R}^m$, allowing to establish an input-output relation: $\Phi = f(\Psi)$, being f the implicit mapping function.

Application phase: the input-output relationship is no longer obtained with explicit formulations, as the ones applied in the data preparation phase. In the application phase the output data is approximated with the mapping function obtained by DL in the training phase. The trained artificial NN, whose training allowed to achieve the implicit mapping function, can be retrained with additional data pairs, generated and gathered from additional CM&B simulations or even from other sources, such as experimental trials. Expletively, relevant supplementary data pairs will allow to enhance the artificial NN and enhance the efficiency and accuracy of the prediction.

4 Literature evolution

This section evaluates the available literature, collecting data from the academic database Web of Science. Peer-reviewed relevant articles were selected for the quantitative analysis presented here. The search in the database was performed using representative keyword combinations, indicated in Table 1, and selecting the "topic/scope" (TS) field in the advanced search. Table 1 shows both the acronyms from the keyword combination and the corresponding total number of papers found for each keyword combination. The acronyms identified in Table 1 for each of the keyword combination are the ones used to refer the corresponding results within Fig.2. The literature search provided a general vision of AI applications in CM&B. From Table 1, it is possible to observe a reduced number of papers combining AI methodologies with CM&B. On the other hand, the combination of FEM with AI methodologies is more relevant, mostly FEM combined with NN.

Fig.2(a) shows the number of papers published per year using the keywords TS-AI, TS-ML, TS-PR, TS-DP, TS-NN and "Finite Element Method" (TS-FEM). This search is independent of the application field. It is not narrowed to CM&B applications. FEM is the most popular discrete numerical method used in CMB&B, therefore, it is relevant to compare the evolution of the number of papers published within the scope of FEM with AI methodologies. Since its development, the number of publications using the FEM increases every year following an exponential growth. As for AI applications, the complexity of FEM's applications strongly depends on the computational capacity. Fig.2(a) shows that FEM's exponential rate becomes even higher from the 1990's forward. This period coincides with the beginning of massive use of personal computers. At the same period, papers dealing with AI methodologies start to slightly increase. However, at that period, only one AI methodology stands-out, showing a strong growth: the artificial NN technique. Between the 2010-2020 period, almost all AI methodologies show an exponential growth, which is explained by the spread of AI to numerous science fields, from financial to social sciences, from molecular dynamics to urban planning. Fig.2(b) shows the number of papers published per year using the keywords TS-AI-CM, TS-ML-CM, TS-PR-CM, TS-DP-CM and TS-NN-CM. It is visible that NN is the preferred AI methodology in computational mechanics and that the number of papers appears to increase only from 2015 forward. On the other hand, combining AI methodologies with biomechanics is more common. Fig.2(c) shows the number of papers published per year using the keywords TS-AI-B, TS-ML-B, TS-PR-B, TS-DP-B and TS-NN-B. It is visible that until 2010 the number of published papers is very modest, however, since 2010 the number of published papers starts to grow significantly, particularly the ones combining ML and NN with biomechanics. Fig.2(d) shows how the number of published papers per year grow combining AI methodologies with the FEM: TS-AI-FEM, TS-ML-FEM, TS-PR-FEM, TS-DP-FEM and TS-NN-FEM. With Fig.2(d) it is possible to observe a solid growth of NN combined with FEM since the early 1990's. It is also visible the fast development of FEM applications combined with ML and DL generic methodologies in the last 5 years.

5 Conclusions

This work does no intends to present a survey or a structured review on AI methodologies for CM&B applications. Instead, it intends to introduce the most basic concepts of AI methodology and show the growth potential in CM&B. It were presented the most suited AI methodologies for CM&B applications and how they interact with each other. Therefore, the chief concepts and ideas behind AI for CM&B were disclosed and the rudiments of ML, PR, DL and DL using artificial NN were introduced. Since ML methodologies using general DL techniques and DL by NN are the most popular in CM&B today, these methodologies were presented with a higher detail, allowing to comprehend the high potential of these techniques to enhance significantly the traditional hard computing techniques used in CM&B.

Regarding the large document search performed in the academic database Web of Science, it was found that AI methodologies present a very high growth rate, regardless the application field. The search revealed that ML methodologies using general DL techniques or DL by NN had an exponential growth in the last 10 years, and from the

observed curves it is expected that such trend will continue in the next years. The search also found that AI methodologies combined with computational mechanics is still in its infancy, with very few works published. However, it is possible to observe that the majority of those work were used ML or DL or NN. Regarding AI methodologies combined with biomechanics, it were found more publications, showing an exponential growth in the last 5 years. It is expected that the topic computational mechanics will follow this trend showing the same exponential growth in the next few years. Regarding the use of AI methodologies with FEM, it was found that DL with NN presents a steady growth since the 1990's and that, in the last 5 years, the number of publications on ML-FEM had an exponential growth.

Table 1 – Total number of articles published until July 2020 within the indicated topic/subject (TS) using the combinations of keywords.

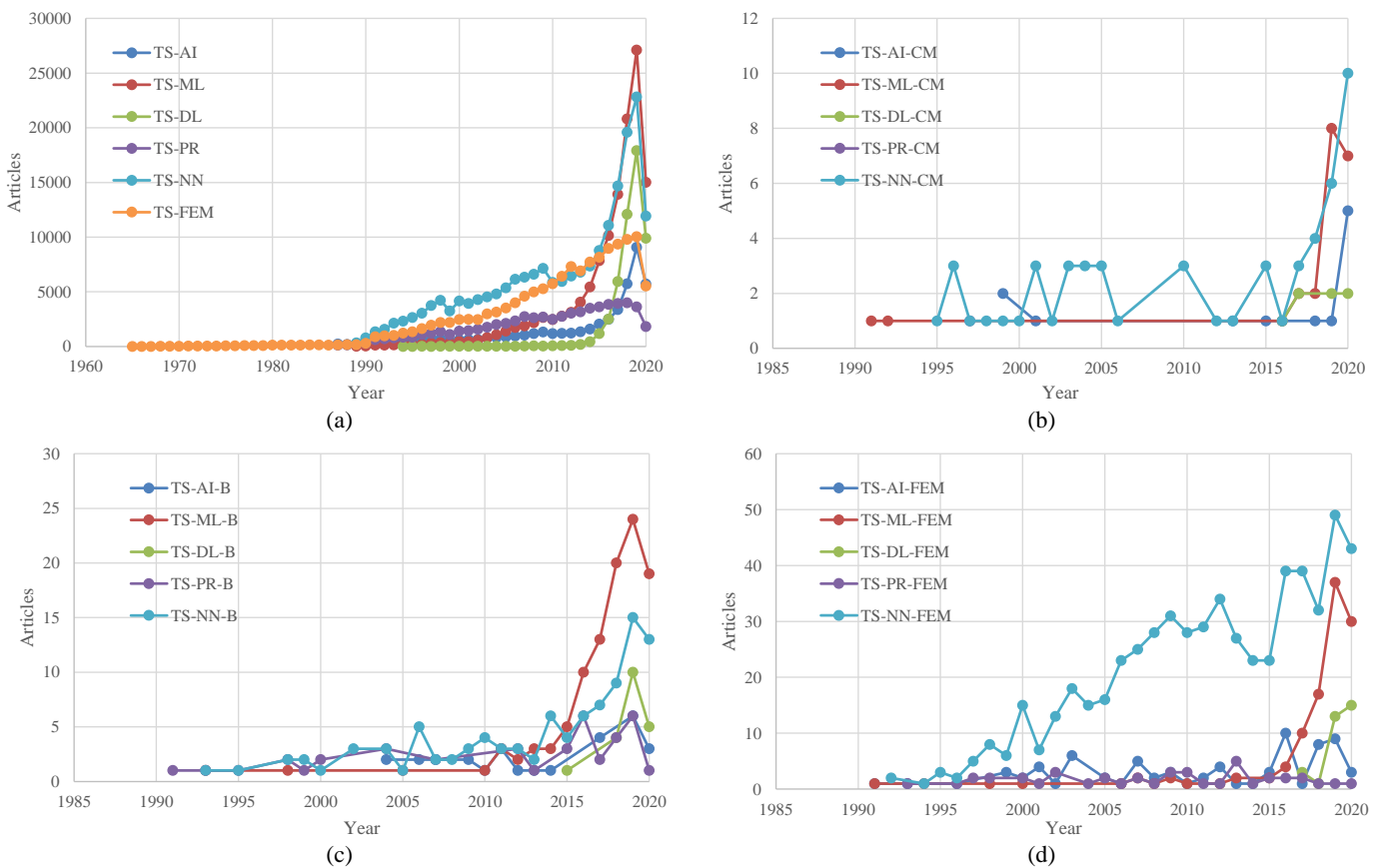| AND	"-"	"Computational mechanics" OR "Structural mechanics"	"Biomechanics"	"Finite element method"
"Artificial Intelligence"	TS-AI: 51009 papers	TS-AI-CM: 13 papers	TS-AI-B: 28	TS-AI-FEM: 75 papers
"Machine learning"	TS-ML: 127898 papers	TS-ML-CM: 22 papers	TS-ML-B: 106 papers	TS-ML-FEM: 114 papers
"Deep learning"	TS-DL: 50593 papers	TS-DL-CM: 7 papers	TS-DL-B: 20 papers	TS-DL-FEM: 32 papers
"Pattern recognition"	TS-PR: 67617 papers	TS-PR-CM: 1 papers	TS-PR-B: 39 papers	TS-PR-FEM: 42 papers
"Neural Networks"	TS-NN: 200218 papers	TS-NN-CM: 54 papers	TS-NN-B: 98 papers	TS-NN-FEM: 584 papers

(a)

(b)

(c)

(d)

Fig.2 – Number of articles published per year within (a) general topic/subject, (b) computational mechanics/structural mechanics topic/subject, (c) biomechanics topic/subject and (d) finite element method topic/subject.

Some relevant works have been published combining ML with CM&B. The already mentioned surveys from Salehi et al. [1] and Oishi et al. [2] are mandatory. Regarding computational mechanics, very recently, ML methodologies were applied to enhance FEM formulation in several fields, such as creating smart elements [16], improving the numerical integration [2] or combined with fracture mechanics [17]. Regarding computational biomechanics, the literature starts to present some promising works. For instances, in [18,19] the authors present a ML combined with the FEM capable to model the mechanical behaviour of human organs, such as breast tissues and liver, in real-time. Such approach can be used in the near future to support clinical practice and real-time surgeries. Up to now, in CM&B, ML has been combined

mostly with FEM. However, there are several other discretization techniques available in the literature, such particle and meshless methods [20], allowing to achieve higher levels of accuracy and discretization freedom.

This work shows that AI is arriving to CM&B. Its inclusion will allow to accelerate the CM&B analyses and to simulate much more complex multiphysics problems, crossing multiple scales and creating new rules, incomprehensible to human intellectual capacity. A paradigm shift is arriving to CM&B.

Acknowledgements

References

[1] Salehi H, Burgueño R, Emerging artificial intelligence methods in structural engineering. Engineering Structures. 2018, 171: 170-189. https://doi.org/10.1016/j.engstruct.2018.05.084

[2] Oishi A, Yagawa G, Computational mechanics enhanced by deep learning. Computer Methods in Applied Mechanics and Engineering. 2017, 327: 327-351. https://doi.org/10.1016/j.cma.2017.08.040

[3] Russell SJ, Norvig P, Canny JF, Malik JM, Edwards DD, Artificial intelligence. A modern approach. vol. 2. Prentice hall Upper Saddle River; 2003. ISBN: 978-0136042594. DOI: 10.1016/j.artint.2011.01.005

[4] Fadlullah ZM, Tang F, Mao B, Kato N, Akashi O, Inoue T, et al. State-of-the-art deep learning: evolving machine intelligence toward tomorrow's intelligent network traffic control systems. IEEE Communications Surveys and Tutorials 2017, 19:2432–55. DOI: 10.1109/COMST.2017.2707140

[5] Noor AK, Potential of Cognitive Computing and Cognitive Systems. Open Engineering. 2015, 5(1):75–88. https://doi.org/10.1515/eng-2015-0008

[6] Pedrycz W, Fuzzy sets in pattern recognition: methodology and methods. Pattern Recognition. 1990, 23:121–46. https://doi.org/10.1016/0031-3203(90)90054-O

[7] Siddique N, Adeli H, Computational intelligence: synergies of fuzzy logic, neural networks and evolutionary computing. John Wiley & Sons; 2013. ISBN:9781118337844. DOI:10.1002/9781118534823

[8] Bezdek,JC, (1994). What is Computational Intelligence? in Computational Intelligence: Imitating Life, ed. J. Zurada, R. Marks and C. Robinson, IEEE Press, Piscataway,1–12. https://doi.org/10.1007/978-3-540-71984-7_1

[9] Daniel T, Casenave F, Akkari N, Ryckelynck D, Model order reduction assisted by deep neural networks (ROM-net). Advanced Modeling and Simulation in Engineering Sciences. 2020, 7:16. https://doi.org/10.1186/s40323-020-00153-6

[10] Wang Y, Cheung SW, Chung ET, Efendiev Y, Wang M, Deep multiscale model learning. Journal of Computational Physics. 2020 406:109071. DOI: 10.1016/j.jcp.2019.109071

[11] Yagawa G, Okuda H, Neural networks in computational mechanics. Archives of Computational Methods in Engineering. 1996. 3:435. https://doi.org/10.1007/BF02818935

[12] Yagawa G, Matsuda A, Kawate H, Neural network approach to estimate stable crack growth in welded specimens. International Journal of Pressure Vessels and Piping. 1995, 63: 303–313. https://doi.org/10.1016/0308-0161(94)00040-P

[13] Oishi A, Yoshimura S, A new local contact search method using a multi-layer neural network. Computer Modeling in Engineering and Sciences. 2007, 21(2): 93–103. DOI:10.3970/cmes.2007.021.093

[14] Kim JH, Kim YH, A predictor–corrector method for structural nonlinear analysis. Computer Methods in Applied Mechanics and Engineering. 2001, 191: 959–974. https://doi.org/10.1016/S0045-7825(01)00296-1

[15] Lopez R, Balsa-Canto E, Onate E, Neural networks for variational problems in engineering. International Journal for Numerical Methods in Engineering. 2008, 75: 1341–1360. https://doi.org/10.1002/nme.2304

[16] Capuano G, Rimoli JJ, Smart fnite elements: A novel machine learning application. Computer Methods in Applied Mechanics and Engineering. 2019, 345: 363–381. https://doi.org/10.1016/j.cma.2018.10.046

[17] Liu X, Athanasiou CE, Padture NP, Sheldon BW, Gao H, A machine learning approach to fracture mechanics problems. Acta Materialia. 2020, 190: 105-112. https://doi.org/10.1016/j.actamat.2020.03.016

[18] Martínez-Martínez F, Rupérez-Moreno MJ, Martínez-Sober M, Solves-Llorens JA, Lorente D, Serrano-Lopez AJ, Martínez-Sanchis S, Monserrat C, Martín-Guerrero JD, A finite element-based machine learning approach for modeling the mechanical behavior of the breast tissues under compression in real-time. Computers in Biology and Medicine. 2017. 90: 116–124. https://doi.org/10.1016/j.compbiomed.2017.09.019

[19] Pellicer-Valero OJ, Rupérez MJ, Martínez-Sanchis S, Martín-Guerrero JD, Real-time biomechanical modeling of the liver using Machine Learning models trained on Finite Element Method simulations. Expert Systems With Applications. 2020, 143: 113083. https://doi.org/10.1016/j.eswa.2019.113083

[20] Belinha J, Meshless methods in biomechanics. Bone tissue remodelling analysis, Springer, 2014. ISBN: 978-3-319-06399-7. DOI: 10.1007/978-3-319-06400-0

Using advanced discretization techniques to simulate the suturing process

Ana Guerra [1], Jorge Belinha [2], Renato Natal Jorge [3]

[1]*aguerra@inegi.up.pt; INEGI, Rua Dr. Roberto Frias, 400, 4200-465; Porto; Portugal*
2 job@isep.ipp.pt; ISEP, Rua Dr. António Bernardino de Almeida, 431, 4249-015; Porto; Portugal
3 rnatal@fe.up.pt; FEUP, Rua Dr. Roberto Frias, 4200-465 Porto, Portugal

Abstract

Wounds or cuts in human skin are very common. Superficial wounds normally heal in short time; however, deep wounds usually required clinical intervention such as sutures to provide the wound closure and timely healing. This process affects the mechanical behaviour of the skin. Advanced discretization techniques, such as finite element method (FEM) and meshless methods can be used to predict the geometry of surgical incisions and to analyse stress and strain distribution in the skin aiming to improve scar formation. In this study we constructed 2D models to simulate the suturing process and to analyse the stress and strain fields obtained, using FEM and natural neighbour radial point interpolation method (NNRPIM) analysis. The simulations' results demonstrated that the highest levels of stress and strain were observed in the area around the wound, in both techniques used. Although this is a preliminary study to estimate the performance of numerical methods in the analysis of stress profile distribution in the human skin, it was possible to conclude that both FEM and NNRPIM are valid tools. Furthermore, the materials used in the simulations were well characterized in terms of elasticity. In the future works, it is intended to refine the model parameters and to include the hyperelastic and the anisotropic behaviour of the human skin.

DOI*: 10.5281/zenodo.4669670*

1 Introduction

Human skin is an important physical barrier between the body and the external environment being the first line of defence against any injury. This organ is composed by three layers. The epidermis (first layer) is very thin and its contribution to the mechanical behaviour of the skin is minimal. The dermis (second layer with approximately 2 mm of thickness) is responsible for the skin's mechanical properties and it provides structural and nutritional support to the skin. The hypodermis (third layer) is mainly composed by fat connective tissue that connects the dermis with the skeletal components. Each skin layer possesses its individual biological structure and its specific mechanical properties [1].

Skin wounds may be a result of traumatic accidents, surgery incisions, burns or due to long periods of immobilization. Superficial skin wounds normally heal in short time; however, deep wound usually required clinical intervention such as sutures to close and avoid blood lose and infection. The suturing process success is based in the surgeon's experience and there is no rigorous protocol to what is right or wrong technique [2]. Accordingly, the use of numerical simulation to analyse the mechanical behaviour of the skin aroused the interest of surgeons. Advanced discretization techniques, such as finite element method (FEM) and meshless methods can be used to predict the geometry of surgical incisions [3] and to analyse stress distribution in the skin [4] in order to reduce scar formation. Stress plays an important role in wound healing and in scar evolution. Accordingly, analyse stress theoretically is demanded, since no invasive or non-invasive technique to measure stress directly is available. This will be very useful in order to minimize negative outcomes such as permanent marks and high stress that reduces blood flow and facilitate the occurrence of hypertrophic scars [5].

In this work, we constructed 2D models simulating the suture process and we performed a linear elasto-static analysis of the stress and strain fields obtaining in each model, using both FEM and Natural Neighbour Radial Point Interpolation Method (NNRPIM). Moreover, the efficiency of both numerical methods used will be addressed.

Corresponding Author:
Ana Guerra
aguerra@inegi.up.pt

2. Methods

2.1. Numerical analysis

FEM and NNRPIM are very useful to simulate biomechanical problems given its possibility to deal with complex geometries, loads and different material properties.

FEM is a mesh-dependent method, in which the domain is discretized with a finite number of interconnected elements forming a mesh. The first step in FEM is to obtain the discretized mesh and then the interpolation function can be reached. The polynomials functions are used to interpolate the field variables over the element. To obtain the discrete equation system, we used the Galerkin method. In order to achieve the global equation system, we need to combine the local element equations for all elements used for the discretization. Accordingly, the global equation system can be solved [6].

In meshless methods, such as NNRPIM, the domain is discretized with a free nodal distribution and the field functions are approximated within an influence-domain rather than an element [7]. In NNRPIM, since there is no predefined nodal interdependency, the nodal connectivity has to be enforced after the nodal discretization. Accordingly, the nodal connectivity is obtained using the natural neighbour concept with the partition of the discretized domain into a set of Voronoï cells. To each one of these cells is associated with only one node [8]. Then the background integration mesh should be constructed. For the numerical integration, NNRPIM uses the Galerkin weak form, being necessary to use a background integration mesh. The integration mesh is obtained using solely the nodal distribution, the previously constructed Voronoï diagram [9]. The Delaunay triangulation is used to subdivided the area of each Voronoï cell in several sub-areas. Finally, the discrete equation system, using the approximation or interpolations shape functions, can be achieved. In NNRPIM, the interpolation shape function combines a radial basis function with a polynomial basis function to obtain the approximation. The interpolation functions possess the Kronecker delta property, which means that the obtained function passes through all scattered points in the influence domain. Accordingly, this property simplify the imposition of the essential boundary conditions [7].

2.2. Solid mechanics

When solids are subjected to loads or forces them become stressed which results in strain, that can be interpreted as deformation or displacement [7]. Solid mechanics is focused in studding the relationship between stress and strain and the relationship between strain and displacements. In this work, only linear elastic materials are considered. It means that the relationship between stress and strain is assumed to be linear and the deformation in the solid caused by loading disappears fully with the unloading. Moreover, all the materials were considered to exhibit isotropic behaviour. For this reason, the materials can be completely defined by its Elastic Modulus (E) and Poisson's ratio (v). Furthermore, the relationship between the components of stress and strain can be given by the Hooke's Law.

The present work was developed in two-dimensions, considering the plane strain or the plane stress assumptions. In this work we aim to analyse the von Mises stress and the equivalent strain obtained in skin. Accordingly, the von Mises stress for each interest point, $\boldsymbol{x}_I$, can be calculated using Eq.(1) and the equivalent strain for each interest point, $\boldsymbol{x}_I$, can also be obtained using Eq.(2). The fully description of all the concepts and formulation in this area is presented in [7].

$$\bar{\sigma}\left(\boldsymbol{x}_I\right) = \sqrt{\frac{1}{2}\left[(\sigma(\boldsymbol{x}_I)_1 - \sigma(\boldsymbol{x}_I)_2)^2 + (\sigma(\boldsymbol{x}_I)_2 - \sigma(\boldsymbol{x}_I)_3)^2 + (\sigma(\boldsymbol{x}_I)_3 - \sigma(\boldsymbol{x}_I)_1)^2\right]} \tag{1}$$

$$\bar{\varepsilon}\left(\boldsymbol{x}_I\right) = \sqrt{\frac{2}{3}\left[(\varepsilon(\boldsymbol{x}_I)_1 - \varepsilon_m)^2 + (\varepsilon(\boldsymbol{x}_I)_2 - \varepsilon_m)^2 + (\varepsilon(\boldsymbol{x}_I)_3 - \varepsilon_m)^2\right]} \tag{2}$$

2.3. Numerical model

In this work, we developed 2D models aimed to simulate the suturing process and to analyse the von Mises stress and the equivalent stain obtained during the process, using FEM and NNRPIM analysis. All the numerical simulations were performed using the software FEMAS. In Fig. 1 the geometry and boundary conditions used are presented. Concerning model A, several points in the boundary were selected and it was applied a force value in each one in order to mimic the stitches made with the needle during suturing in the area around the wound, as illustrated in Fig. 1. In the following models (B, C and D) more specific points were consecutively selected and a similar force was applied in each one, as illustrated in Fig. 1. In Table 1 the model dimensions and the material properties of each skin layer used to constructed the models are presented.
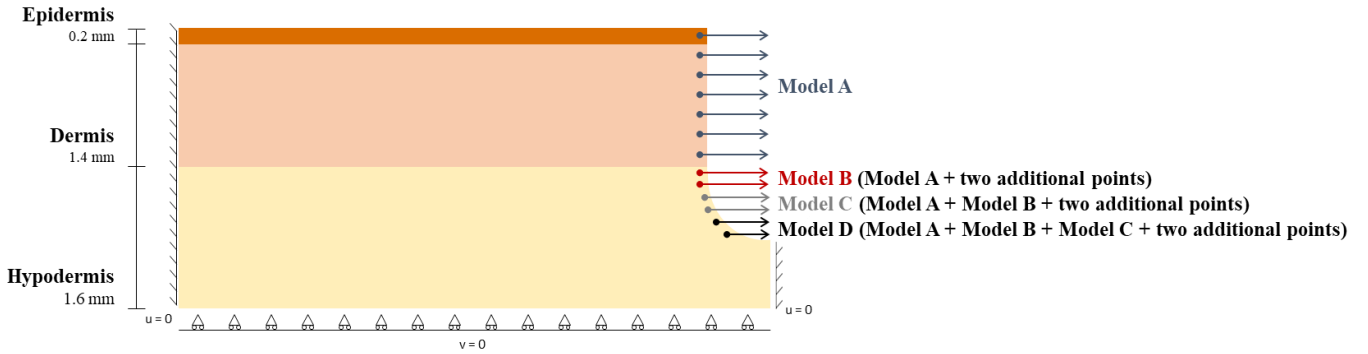
Fig. 1 - Model geometry and boundary conditions for model A, model B, model C and model D.

Table 1 - Model dimensions and material properties [10, 11].

Skin layer	Elastic Modulus (E) - MPa	Poisson's coefficient (v)
Epidermis	102	0.48
Dermis	10.2	0.48
Hypodermis	0.0102	0.48

3. Results

In this section, we will only present the results obtained in the hypodermis. In epidermis and dermis the stress and strain fields achieved were very high and homogeneous related to the same layer. The results obtained for the von Mises stress for model A, in which it was applied a force in the boundary of epidermis and dermis in order to simulate the suturing process, are presented in Fig. 2. Analysing the von Mises stress isomaps (Fig. 2(a)) it is possible to observe that the highest stress levels (around 8×10^{-3} MPa) were obtained in the surrounding wound area and in the transition from the hypodermis to the dermis, in FEM and NNRPIM analysis. The measurement of this parameter in specific points around the wound (Fig. 2(b)) confirms this observation.
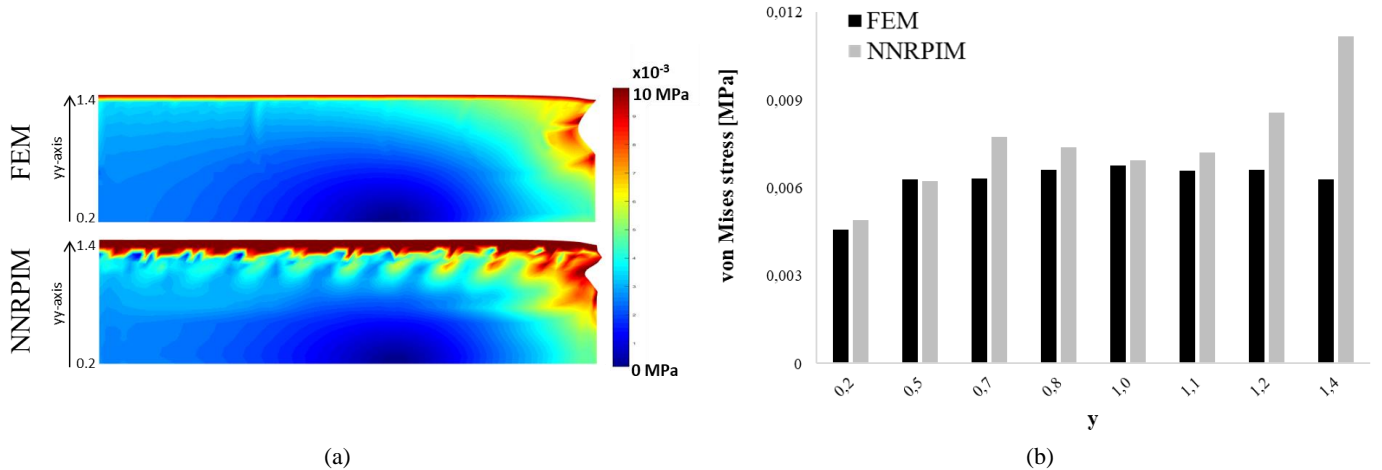

(a)   (b)

Fig. 2 - (a) von Mises stress isomaps obtained with FEM and NNRPIM for model A; (b) von Mises stress measured in specific points in the area around the wound, in the two advanced discretization techniques.

The results obtained for the equivalent strain for the same model are presented in Fig. 3. Analysing the equivalent strain isomaps (Fig. 3(a)) and the graph (Fig. 3(b)) it is possible to observe that the highest strain levels, around 0.6, were obtained in the area around the wound, in FEM and NNRPM analysis.

The results obtained for the von Mises stress for model B, in which it was applied a force in the boundary of epidermis, dermis and hypodermis in order to simulate the suturing process, are presented in Fig. 4. Analysing the von Mises stress isomaps (Fig. 4(a)) and the graph (Fig. 4(b)) it is possible to observe that the highest stress levels (around 8×10^{-3} MPa)

were obtained in the surrounding wound area, in FEM and NNRPIM analysis. It was also obtained high von Mises stress levels in the transition from the hypodermis to the dermis (Fig. 4(a)).

The results obtained for the equivalent strain for the same model are presented in Fig. 5. Analysing the equivalent strain isomaps (Fig. 5(a)) and the graph (Fig. 5(b)) it is possible to observe that the highest strain levels, around 0.8, were obtained in the area around the wound, in both advanced discretization techniques used.
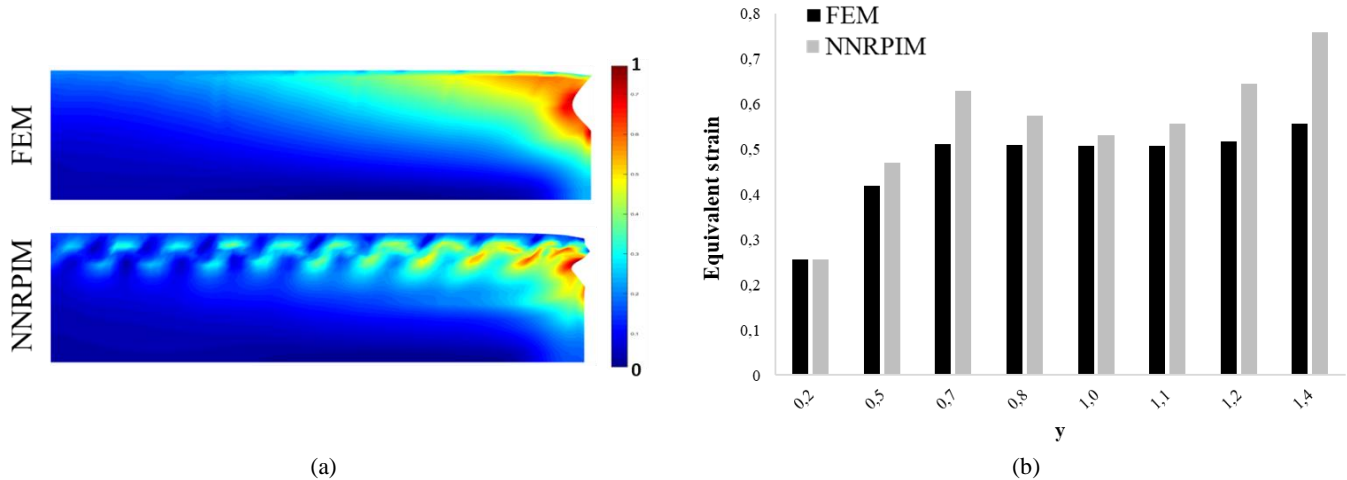

(a)   (b)

Fig. 3 - (a) Equivalent strain isomaps obtained with FEM and NNRPIM for model A; (b) Equivalent strain measured in specific points in the area around the wound, in the two advanced discretization techniques.
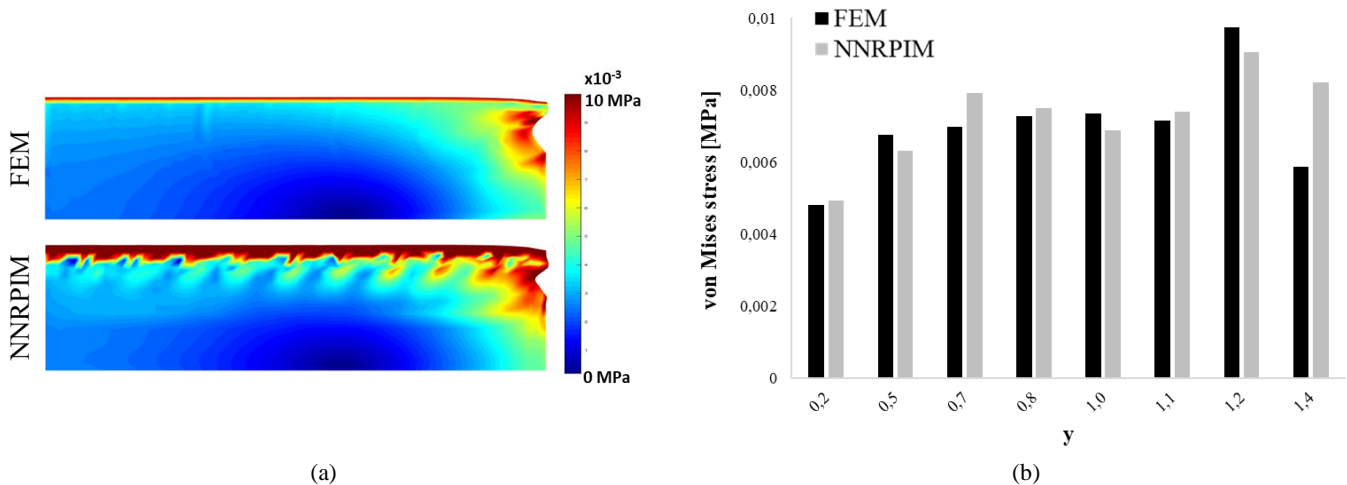

(a)   (b)

Fig. 4 – (a) von Mises stress isomaps obtained with FEM and NNRPIM for model B; (b) von Mises stress measured in specific points in the area around the wound, in the two advanced discretization techniques.

The results obtained for the von Mises stress for model C, in which it was consecutively applied a force in more points in the boundary of hypodermis in order to simulate the suturing process, are presented in Fig. 6. Analysing the von Mises stress isomaps (Fig. 6(a)) and the graph (Fig. 6(b)) it is possible to observe that the highest stress levels (around 9×10^{-3} MPa) were obtained in the surrounding wound area, in FEM and NNRPIM analysis. Once again, it was also obtained high von Mises stress levels in the transition from the hypodermis to the dermis (Fig 6(a)).

The results obtained for the equivalent strain for the same model are presented in Fig. 7. Analysing the equivalent strain isomaps (Fig. 7(a)) and the graph (Fig. 7(b)) it is possible to confirm that the highest strain levels, around 0.8, were obtained in the area around the wound, in FEM and NNRPIM analysis.

The results obtained for the von Mises stress for model D, in which it was consecutively applied a force in more points filling in the entire wound, are presented in Fig. 8. Analysing the von Mises stress isomaps (Fig. 8(a)) and the graph (Fig. 8(b)) it is possible to observe that the highest stress levels (around 8×10^{-3} MPa) were obtained in the surrounding wound area, in FEM and NNRPIM analysis. Moreover, it was also obtained high von Mises stress levels in the transition from

the hypodermis to the dermis, in the both techniques used. Analysing the advanced discretization techniques solution isomaps (Fig. 8(a)) it is also possible to observe that the wound is practically closed.
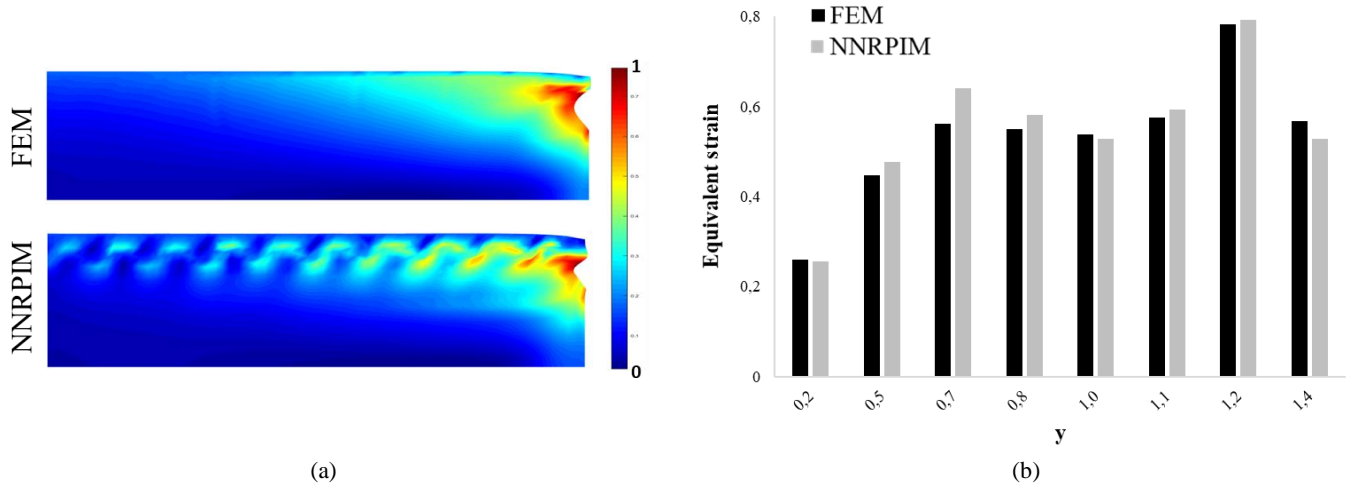

(a)   (b)

Fig. 5 - (a) Equivalent strain isomaps obtained with FEM and NNRPIM for model B; (b) Equivalent strain measured in specific points in the area around the wound, in the two advanced discretization techniques.
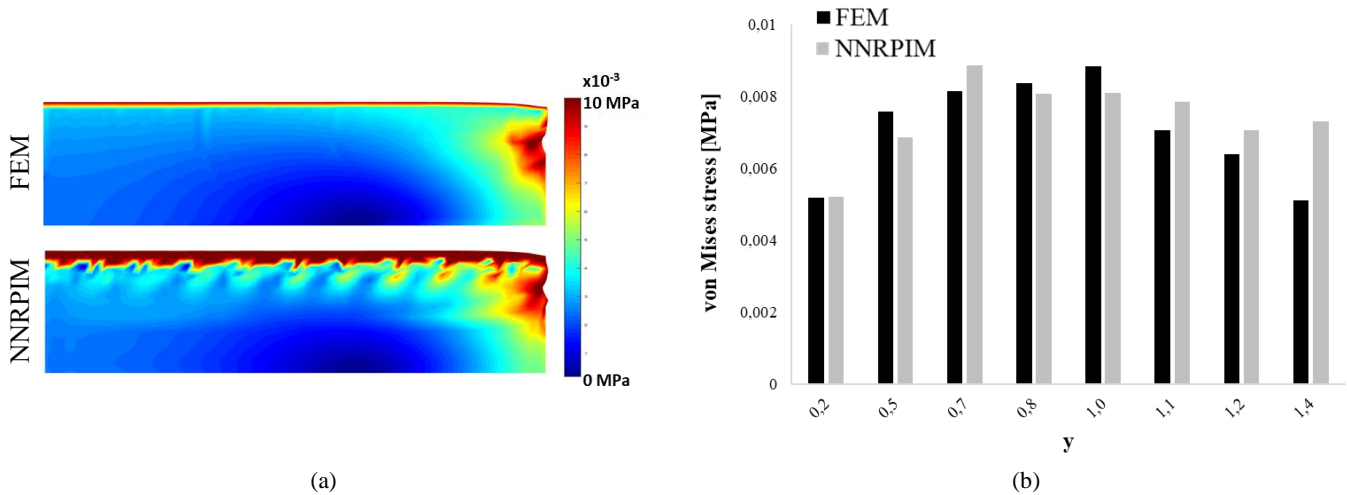

(a)   (b)

Fig. 6 - (a) von Mises stress isomaps obtained with FEM and NNRPIM for model C; (b) von Mises stress measured in specific points in the area around the wound, in the two advanced discretization techniques.

The results obtained for the equivalent strain for the same model are presented in Fig. 9. Analysing the equivalent strain isomaps (Fig. 9(a)) and the graph (Fig. 9(b)) it is possible to observe that the highest strain levels, around 0.8, were obtained in the area around the wound, in both advanced discretization techniques used.

4. Discussion and Conclusions

Computational models are very useful to simulate mechanical and biochemical problems in order to improve humans' health. FEM is a powerful numerical method that allows to deal with irregular boundaries, general loads, nonlinear problems, different materials and boundary conditions, it permits to create meshes with variable element size and it is easy to modify and dynamic [12]. Comparatively to FEM, meshless methods have the re-meshing efficiency, which allows to deal with large distortions of soft materials, such as the skin [7]. Moreover, these methodologies are less expensive and time consuming when compared with the experimental ones.

In this work, FEM and NNRPIM analysis were used to study the stress and strain fields obtained in the skin during the suturing process. In our models, the highest levels of stress (around 8×10^{-3} MPa) and strain (around 0.8 and 0.6) were obtained in the area around the wound. Moreover, high levels of stress were also obtained in the transition between the hypodermis and the dermis. In models C and D, in the end of the simulations, the wound is practically closed. We are

11

aware that the mechanical properties of the healthy and wounded skin tissue are different. However, the aim of this work was to analyse the stress and strain fields obtained in all the skin layer when the suture occurs. Therefore, we only used the mechanical properties related to healthy skin.
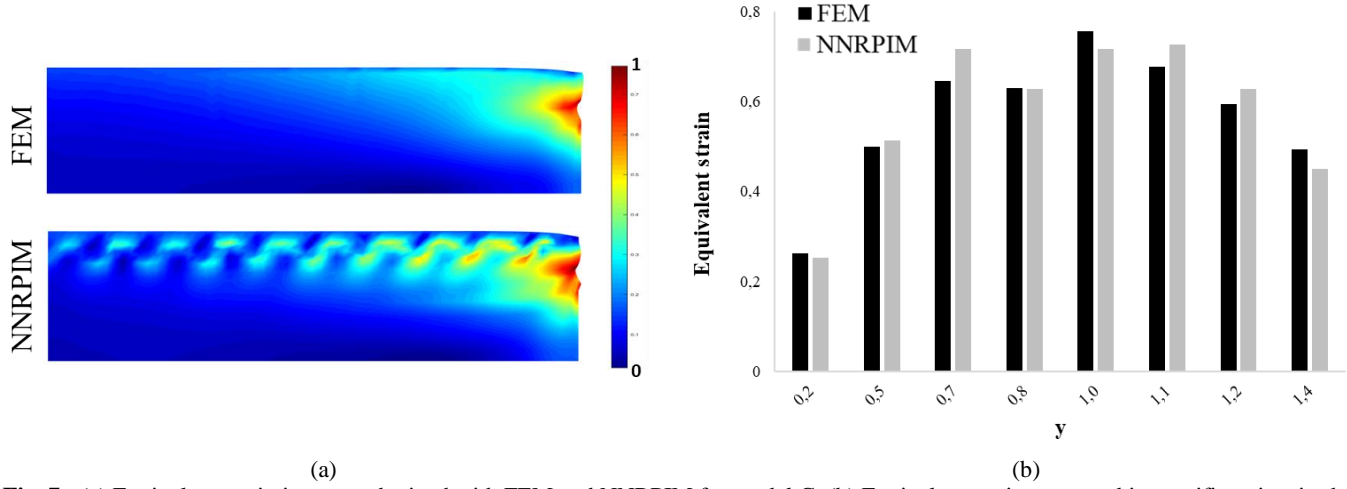

(a)　　　　　　　　　　　　　　　　　　　　　　　　　　　　(b)

Fig. 7 - (a) Equivalent strain isomaps obtained with FEM and NNRPIM for model C; (b) Equivalent strain measured in specific points in the area around the wound, in the two advanced discretization techniques.
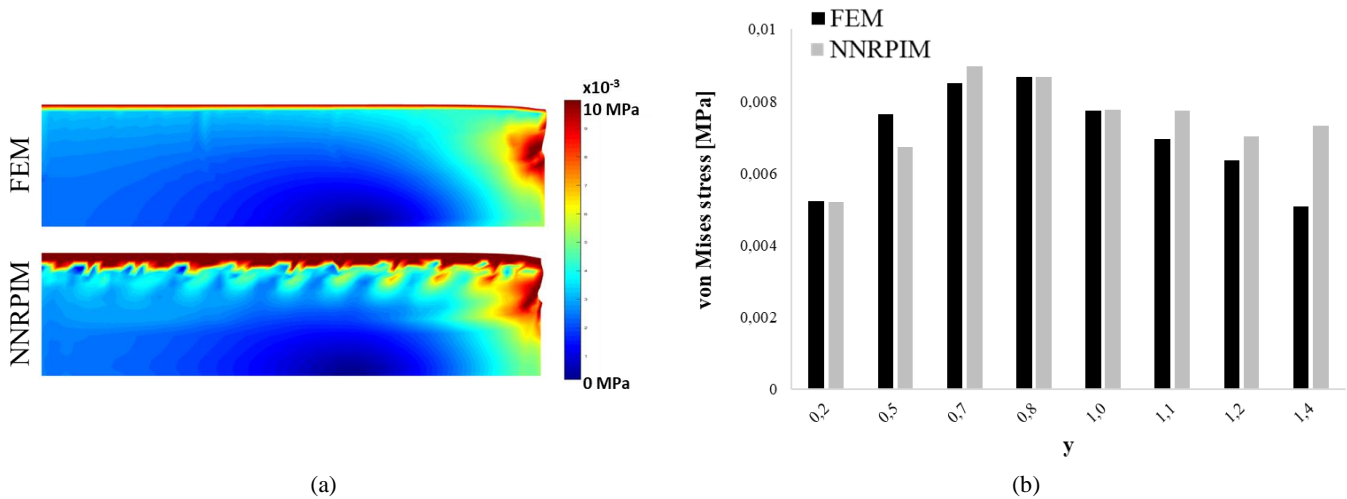

(a)　　　　　　　　　　　　　　　　　　　　　　　　　　　　(b)

Fig. 8 - (a) von Mises stress isomaps obtained with FEM and NNRPIM for model D; (b) von Mises stress measured in specific points in the area around the wound, in the two advanced discretization techniques.

Human skin exhibits nonlinear stress-strain, anisotropic and viscoelastic characteristics [13]. Nevertheless, in order to decrease the model's complexity, most of the studies assume skin as an isotropic and linear elastic material [14]. Accordingly, in this study the skin was modelled as an isotropic and linear elastic material.

Although this is a preliminary study to evaluate the performance of these numerical methods in the analysis of stress profile in human skin it was possible to conclude that FEM and NNRPIM are valid numerical tools. The numerical methods used in the simulations demonstrated equivalent results. Moreover, the materials used in the simulations were well characterized in terms of elasticity. In the future, it is intended that this kind of models could assist surgeons during surgery planning in order to recognize the regions of stress and strain concentration to improve the healing of sutured wounds. Despite the simplifications, the wound closure model presented in this paper is a useful tool for evaluating the merits of different excision shapes and improving the healing of sutured wounds.

Acknowledgements and Funding

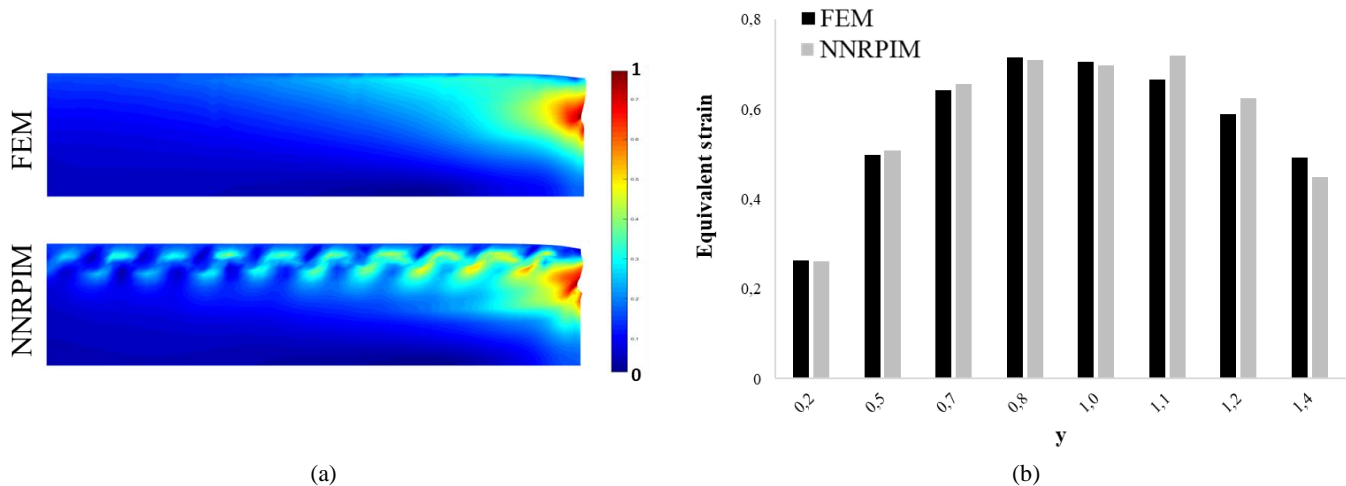(a)   (b)

Fig. 9 - (a) Equivalent strain isomaps obtained with FEM and NNRPIM for model D; (b) Equivalent strain measured in specific points in the area around the wound, in the two advanced discretization techniques.

References

[1]   Reihsner R, Balogh B, Menzel EJ. Two-dimensional elastic properties of human skin in terms of an incremental model at the in vivo configuration. Med Eng Phys. 1995;17(4):304-13.

[2]   Flynn C. Finite element models of wound closure. J Tissue Viability. 2010;19(4):137-49.

[3]   Wang P, Becker AA, Jones IA, Glover AT, Benford SD, Greenhalgh CM, et al. Virtual reality simulation of surgery with haptic feedback based on the boundary element method. Computers & Structures. 2007;85(7):331-9.

[4]   Yang C, Tang D, Haber I, Geva T, del Nido PJ. In vivo MRI-based 3D FSI RV/LV models for human right ventricle and patch design for potential computer-aided surgery optimization. Computers & Structures. 2007;85(11):988-97.

[5]   Cavicchi A, Gambarotta L, Massabò R. Computational modeling of reconstructive surgery: The effects of the natural tension on skin wrinkling. Finite Elem Anal Des. 2009;45(8):519-29.

[6]   Fish J, Belytschko T. A First Course in Finite Elements: John Wiley & Sons; 2007.

[7]   Belinha J. Meshless Methods in Biomechanics - Bone Tissue Remodelling Analysis: Springer International Publishing; 2014.

[8]   Belinha J, Dinis LMJS, Jorge RMN. The analysis of the bone remodelling around femoral stems. Math Comput Simul. 2016;121(C):64-94.

[9]   Dinis LMJS, Natal Jorge RM, Belinha J. Analysis of 3D solids using the natural neighbour radial point interpolation method. Comput Methods Appl Mech Eng. 2007;196(13):2009-28.

[10] Areias P, Natal Jorge R, Barbosa J, Fernades A, Mascarenhas T, Oliveira M, et al. Experimental and Finite Element Analysis of Human Skin Elasticity2003.

[11] Li C, Guan G, Reif R, Huang Z, Wang R. Determining elastic properties of skin by measuring surface waves from an impulse mechanical stimulus using phase-sensitive optical coherence tomography. Journal of the Royal Society, Interface / the Royal Society. 2011;9:831-41.

[12] Belinha J, Dinis LMJS, Natal Jorge RM. The analysis of the bone remodelling around femoral stems: A meshless approach. Math Comput Simul. 2016;121:64-94.

[13] Silver FH, Freeman JW, DeVore D. Viscoelastic properties of human skin and processed dermis. Skin Res Technol. 2001;7(1):18-23.

[14] Zahouani H, Pailler-Mattei C, Sohm B, Vargiolu R, Cenizo V, Debret R. Characterization of the mechanical properties of a dermal equivalent compared with human skin in vivo by indentation and static friction tests. Skin Res Technol. 2009;15(1):68-76.

Artificial Neural Networks Applied in Mechanical Structural Design

J.P.A. Ribeiro[1], L.F.F. Gomes[2], S.M.O. Tavares[1]

[1] *Faculty of Engineering, University of Porto, Rua Dr. Roberto Frias, 4200-465, Porto, Portugal, {jp.ar@hotmail.com; sergio.tavares@fe.up.pt}*
[2] *University of Minho, Campus de Gualtar, 4710-057, Braga, Portugal, luisgomes24.97@gmail.com*

Abstract

Artificial Intelligence has brought many new problem-solving approaches to society in the last few years. In Artificial Intelligence domain, the Machine Learning techniques are being very successful mainly because of their ability to learn. The main objective of this article is the research, development and application of Artificial Intelligence techniques for mechanical structural design. Selected method is based on the Artificial Neural Networks, that allows the prediction of a certain variable based on a given set of data. The applied artificial network was developed in Python with TensorFlow library and the database was prepared using the finite element software, Ansys, with parametric language for automatic data extraction. A classic solid mechanics case study, comprising a plate with a central hole subjected to uniaxial remote stress, is explored. It is intended to obtain the stress distribution for a plate with hole radius between 25 and 50 mm. With Artificial Neural Networks, a substantial reduction in the simulation time is observed, being, approximately, 79 times faster when compared to the solution time of the conventional finite element approach. The developed neural network has a relative average error of about 4.57%, which is considered satisfactory given that it is a first application of these networks in this domain. In conclusion, with this work it is possible to highlight the potential advantages of Artificial Neural Networks in applied to stress/strain calculation in solid mechanics: shorter response time, less computational resources and problem simplification, in detriment of a lower resolution/accuracy of structural behaviour. Optimization procedures and digital-twin concepts can take advantage of these benefits, enabling near real-time calculations.

1. Introduction

Artificial Intelligence (AI) is becoming increasingly present in our daily lives. The benefits that it has brought to society in recent years are remarkable. Its use in daily complex life tasks, like autonomous driving, prove that the human being has more and more confidence in this kind of solutions. The success of AI models in the last few years is closely related to their ability to learn. The models with this property enable the development of Machine Learning (ML) approaches, allowing its exploitation in a wide range of engineering problems.

In a computer program, it is specified to the computer what it is expected to do when some input is presented. On the other hand, in ML systems, instead of programming the actions, they are learned using data of the specific problem that is intended to solve. With the advances in computer architectures and the good results shown by ML technologies, there is a growing interest in the scientific community on this topic. Efforts are being made to expand the AI areas of application and to improve its performance even more and to take advantage of its capabilities.

The purpose of this article is to study, develop and apply AI techniques, namely Artificial Neural Networks (ANNs), in the mechanical design. The specific case study will be the classical problem of a plate with central hole under uniaxial tension. In this way, it is intended, through ANNs, to predict the plate stress field and compare it with the stress field obtained from Ansys software based on the finite element method. The comparison terms are the model accuracy, the computational costs and the simulation time.

2. Artificial Neural Networks

Connectionist Systems, more commonly referred to as ANNs, are ML models inspired by the human neurological system. Perhaps the first ANN architectures were made to simulate the human brain, they have become powerful tools to solve a great variety of problems. One of the most popular tasks performed by these models is pattern recognition. For

this purpose, it is given to the network input-output pairs, and then it will try to find a function that correctly approximates the real relations between them. In a simplified way, an ANN can be defined as presented in Eq.(1), assuming f^* as the real relationship between x and y. The function f is defined with the choice of the ANN architecture. The learning process will determine the values of $\boldsymbol{\theta}$ [1].

$$\hat{y} = f(x, \theta) \tag{1}$$

where $\boldsymbol{x}$ represents the input data, $\boldsymbol{\hat{y}}$ the predicted output data, f the approximate function of f^* and $\boldsymbol{\theta}$ the learning parameters.

The most popular ANN architecture is the feed-forward neural network, also called Multilayer Perceptron (MLP). In this architecture, the information flows in only one direction, from the input layer, passing through the hidden layers and ending in the output layer. Each computational node in an ANN is called a neuron. Fig.1 shows an example of the MLP architecture.
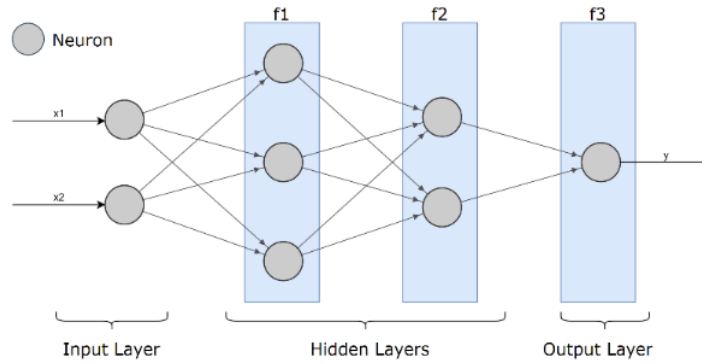

Fig.1 - Representative example of an ANN.

When an ANN has more than one hidden layer, it can be called Deep Neural Network (DNN), since the information is treated hierarchically, in layers with different depths. From Fig.1, one can rewrite the ANN definition, assuming that the f function in Eq.(2) is the composition of n functions, where n represents the number of computing layers in the network [1],[2].

$$\hat{y} = f_3(f_2(f_1(x, \theta_1), \theta_2), \theta_3) \tag{2}$$

where f_i and θ_i represent the approximate function and the learning parameters of layer i, respectively.

The presented layers in Fig.1 are fully connected, which means that each neuron receives information from all the nodes in the previous layer, and its output is used from every neuron in the next layer.

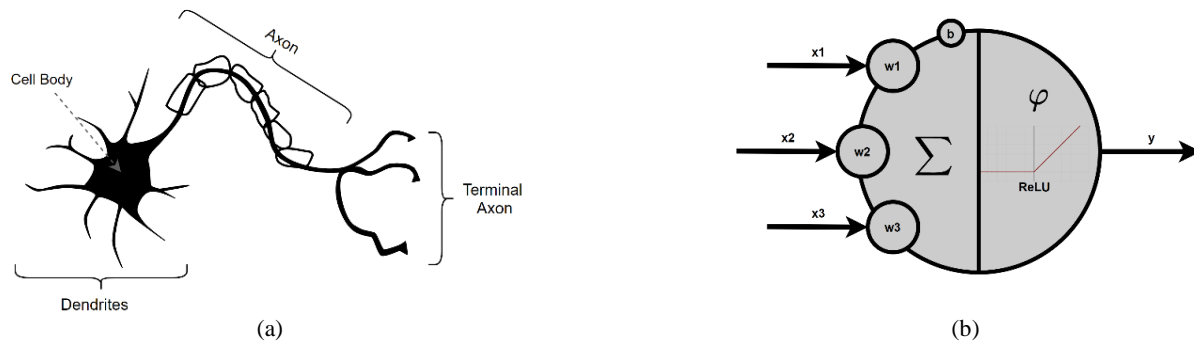(a)   (b)

Fig.2 – Comparison between natural and artificial neurons: (a) the natural neuron receives information through the dendrites, processes it in the cell body and sends it to adjacent neurons through the axon; (b) The artificial neuron receives information from other neurons (x_i), processes it ($\sum$ and φ) and sends the result (y) to other nodes.

The artificial neuron structure is an attempt to reproduce the human nerve cell as presented in Fig.2. The neuron receives information, processes it, and then forwards it to adjacent nodes. The process of transmitting information is called a synapse. In the artificial neuron, the information is processed in two stages. The first stage is a weighted sum of all the input data and the second is performed by an activation function, that decides if the neuron is activated or not, *i.e.* if the information will pass to adjacent neurons [3]. The activation function (φ) maps the weighted sum from the]-∞; +∞[interval to the desired domain. One of the most popular activation functions is the Rectified Linear Unit (ReLU), which has an output domain of [0, +∞[, activating the neuron only when the input is greater than 0 [4]. In the learning process, at the neuron level, the learning parameters are the weights from the input connections and the bias, defined as b. The bias is an additional parameter to improve the flexibility of neural networks.

$$y = ReLU(w1 \cdot x1 + w2 \cdot x2 + w3 \cdot x3 + b) \tag{3}$$

where x_i and w_i are the input data from the neuron i of the previous layer and its associated weight, b is the bias and y represents the processed information. The *ReLU* function is defined in Eq.(4).

$$ReLU(x) = \max(0, x) = \begin{cases} 0, & if\ x < 0 \\ x, & if\ x \geq 0 \end{cases} \tag{4}$$

The learning process is a loop, starting with all the weights set with random values, being adjusted in every iteration. Each iteration has two stages: the forward propagation, where the input data (x) is used to predict the output value ($\hat{y}$); and the weights update, using the back-propagation algorithm to calculate the error gradient for each layer, propagating it from the output to the other layers [5]. This process is determined by two main elements: the loss function and the optimizer. The loss function defines a measurement of the network success in its task during the learning iterations. It uses the results predicted ($\hat{y}$) by the network in each step and the real values (y) to calculate the error. One of the most used loss functions in regression models is the Mean Square Error (MSE) defined in equation Eq.(5).

$$MSE(y, \hat{y}) = \frac{1}{n}\sum_{i=1}^{n}(y_i - \hat{y}_i)^2 \tag{5}$$

where n is the number of data samples. The main goal is to minimize the loss function. Using the error gradient, the ANN must converge to its minimum. The optimizer defines the way that the weights in the network are updated based on the gradient calculated with the back-propagation algorithm. The optimizers implement some variant of stochastic gradient descent (SGD). Some of the most popular optimizers for regression problems are *RMSProp* and *Adam* [1],[2].

3. Plate with Central Hole

The case study is a classic example of structural mechanics, namely a plate with a central hole subjected to uniaxial remote stresses [6],[7]. The plate variables are length plate *L*, width *W*, thickness *t* and the hole diameter, which is characterized by *d*, as seen in Fig.3. Other case studies can be found in [8].

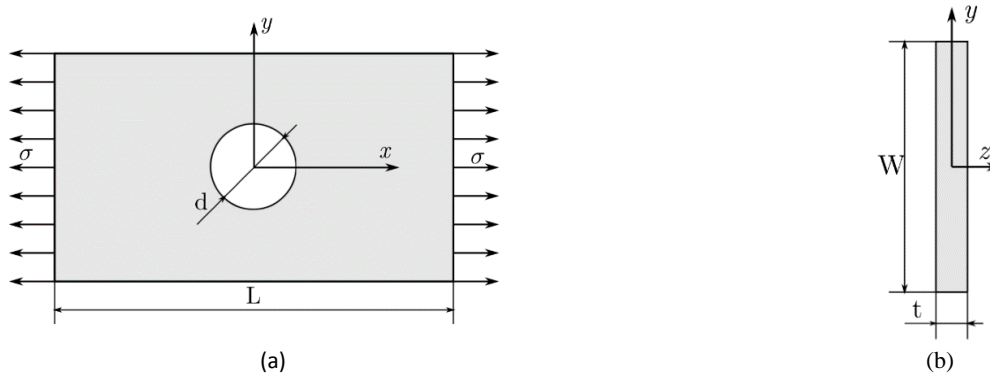(a)   (b)
Fig.3 - Plate with central hole: (a) front view; (b) side view.

Thickness is much smaller than the other dimensions. Thus, a 2D analysis is performed, assuming a plane stress state case. Furthermore, the plate is symmetrical about the axes, so the problem can be simplified by analysing only a quarter of the plate, where *l* is half of the length, *w* half of the width and *r* the plate hole radius.

3.1. Problem Definition

Finite Element Software such as Ansys Mechanical calculates the stress/strain distributions efficiently, even in complex structures. However, this method requires large computational resources, and the time for generation of a regular finite element mesh and the time required for matrix calculation may be too long. Furthermore, whenever a boundary condition or material property changes, it is necessary to simulate again. All of this leads to a high computational cost, both in terms of necessary resources and in terms of time spent on mechanical design activities. With the advances in deep learning algorithms, it is possible to perform the same type of analysis of stress distribution using ANN. This new approach reduces the computational cost because the process is faster, introducing only an approximation error [9]. Thus, this research intends to determine the stress field using ANN. Table 1 shows the main properties of the problem, namely the geometric properties, the material properties and the request load value applied at the ends of the plate.

Table 1 - Problem properties: plate with central hole.

Variables	l (mm)	w (mm)	r (mm)	E (GPa)	v	σ (MPa)
	250	125	25/50	210	0.3	100

4. Methodology

Firstly, it is evaluated what it is intended to be predicted (output variable) and which variables affect the result (input variables). Then, it is created a database, where a set of values of the input and output variables are collected for different cases. These data are obtained with the Ansys Mechanical software. Finally, the entire structure of the ANN is built and applied to the case under study, where the Python language and the Keras library are used. As the material and geometric properties and the loading stress were considered constants, and only the value of *r* is variable. The variation of the stress field between each simulation is characterized by the radius variation. In addition, a stress field is formed by a group of normal stresses calculated on a set of points. Thus, the normal stress depends on the position of the plate point, which it is characterized by the respective Cartesian coordinates. Therefore, the ANN output variable is the normal stress and the input variables are the *x* and *y* coordinates and the hole radius value, as shown in Fig.4.
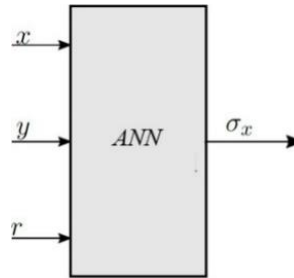

Fig.4 – ANN scheme.

4.1. Database

The database is formed by a set of CSV files (Comma-Separated Values), which present the *x* and *y* coordinates of the nodes that make up the finite element model mesh and the respective normal stress values, calculated in Ansys on those same nodes, for a given *r*, as shown in Fig.5 (a). Although quadratic quadrilaterals elements are used, only the values of calculated stresses in the corner nodes were registered in the database. The radius of the plate hole are between 0.1 to 62.5 mm, where the increment value between each simulation is 1.25 mm, except for the first one. Thus, 51 simulations are performed in Ansys, to obtain the data associated with each value of *r*, as shown in Fig.5 (b).

The database is built in two main steps. The first step is the automatic extraction of the stress values for a given value of *r*, using an APDL Command (Ansys Parametric Design Language). The second step, on the other hand, allows the set of simulations necessary for this analysis to be carried out automatically, and it is not necessary to simulate individuality whenever the value of *r* is changed. This procedure is performed through scripting.

4.2. Data Analysis

An initial data analysis was performed to better evaluate the problem. All the data from the different CSV files was gathered, Fig.5 (b), in a single file, Fig.5 (c). This procedure was performed with the support of the Python Pandas library.

With the structured data, box diagrams for each variable are represented and evaluated, Fig.6. This type of representation allows a better understanding of how the data is distributed.
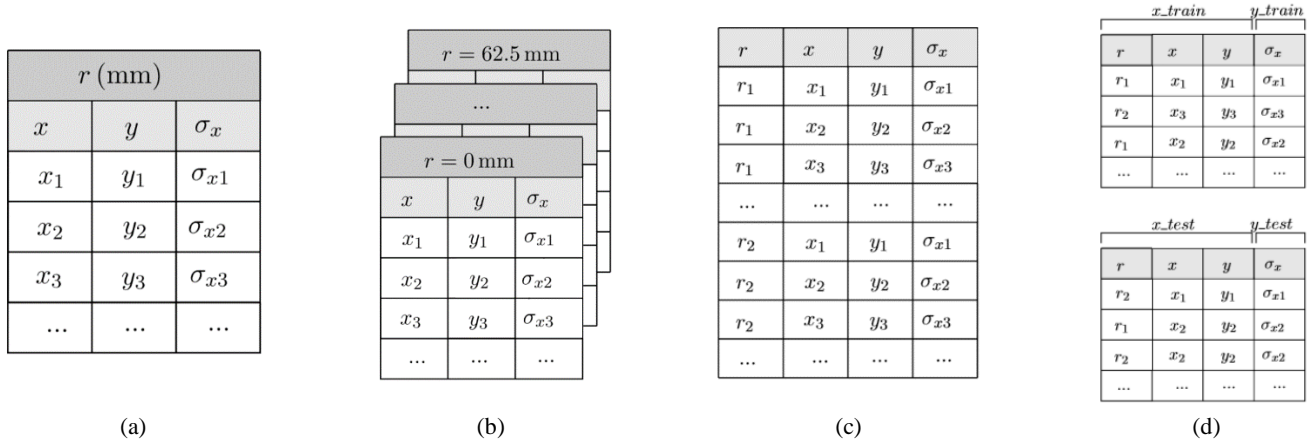

Fig.5 – Database: (a) for a given value of *r*; (b) for the 51 values of *r*; (c) all data; (d) data splitting.

4.3. Data Pre-processing

Data pre-processing is required to homogenize the data, increasing the effectiveness of the ANN. For the case under study, since that all input data are similar in size, it is used the original data. In addition, it is necessary to divide the data into two groups: training data and testing data. Data splitting is done through Python's Scikit-learn library. In Fig.5 (d) it is graphically represented this division. This division is performed through the *train_test_split* function that divides the data in a random way. For the case under study, 80% of the data corresponds to the training data and the remaining 20% to the testing data.
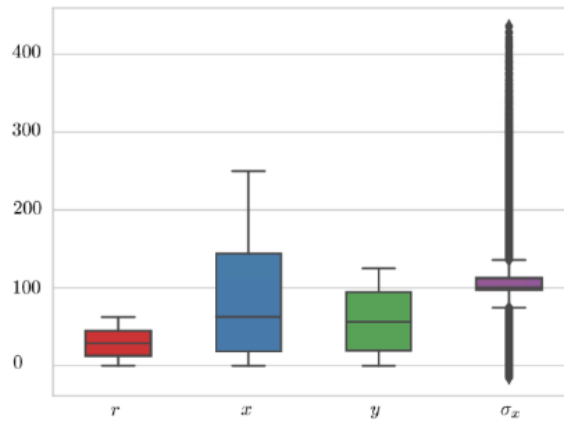
Fig.6 - Box diagrams: *r*, *x*, *y* and σ_x.

4.4. Model Construction

The construction of the ANN model is performed using the Sequential model. The model is formed by six fully connected layers and an output layer that allows obtaining single continuous values. In all layers, except for the last one, the activation function is *ReLU*. In the first layer 128 neurons are used and presented three input variables in vector form. Then, two more layers are used with 128 neurons, one with 64, one with 32 and another with 16. Finally, there is a layer with only 1 neuron that corresponds to the output variable. Fig.7 shows the graphical representation of the ANN, obtained through the ANN Visualizer library.

After built the model, the training configuration is defined. For this, the compile method is used. The optimizer chosen is *RMSProp*. The evaluation metrics are the Mean Absolute Error (MAE), the Mean Square Error (MSE) and the Mean Absolute Percentage Error (MAPE). The chosen loss function is MSE.
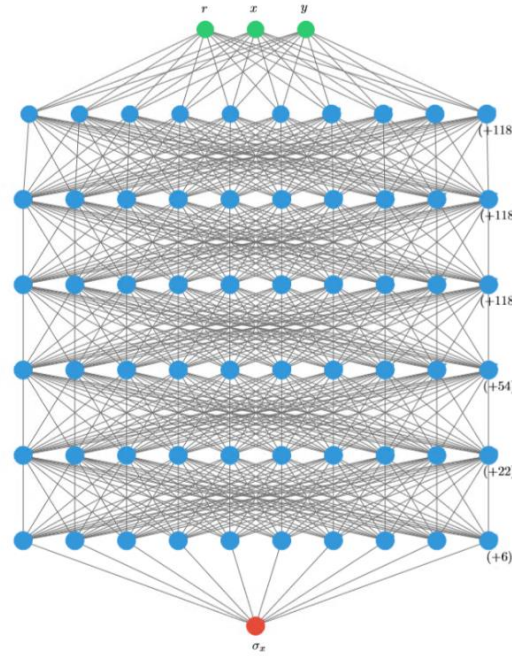

Fig.7 - Representation of the ANN to predict σ_x.

4.5. Train the Model and Evaluation

For model training, the *fit* method is adopted, which allows training the network for a given number of epochs. Note that an epoch corresponds to the time when all training data is processed only once. For the case under study, data stored in *x_train* matrix are used as input data, and data stored in *y_train* as output data. Also, training data is divided using the *validation_split* function, which is used as validation data. For the case under study, 20% of the training data are defined for validation purposes. In addition, it is required to evaluate the number of seasons for model training. In this case, a maximum value of 500 epochs is defined. *Batch_size* is the size of the training sample subset, which will be used during the training process of the network. For the case under study, it is defined a *batch_size* of 20. Finally, callbacks are used to improve the performance of the neural network. Two types of *callbacks* are used: *EarlyStopping* and *TensorBoard*. *EarlyStopping* stops training when a specific monitored metric stops to improve for a specified number of epochs, previously defined with the *patience* argument. As it is intended to decrease the loss function, the metric chosen to be monitored is *val_loss*. Furthermore, 20 epochs are attributed to the *patience* argument. On the other hand, *TensorBoard* is a visualization tool that allows representing and saving the metrics defined according to the epochs. Thus, it is possible to achieve a straightforward visualization of the ANN best configuration.

Fig.8 shows the evolution of MAE, MAPE and MSE along the epochs. As noted, the ANN only required 75 epochs to train. Both, for training and validation, the value of the three metrics decreases as the number of epochs increases. Since that the loss function is the same as the MSE metric, it also decreases as the amount of epochs increases.

After the ANN is trained, test data is evaluated, using the *evaluate* method. With this method and for the case under study, the values of the metrics are: *loss = 10.88; mae = 2.18; mse = 10.88; mape = 6.34*. As noticed, the metrics show good results, which means that the network is forecasting correctly.

5. Results

The *predict method* is used for normal stress calculation (output variable), considering the input variables, previously presented. For this case study, it is intended to obtain the stress distribution, σ_x, for a plate with a central hole of radius *r*. Thus, through the ANN it is possible to predict the stress values necessary to build the stress map. This forecast is made for a plate with radius hole between 25 and 50 mm. To obtain the stress field, it is necessary to estimate the stress

value in a set of points. 873 and 829 points are used for the radius 25 and 50 mm, respectively. The *x* and *y* coordinates are obtained through the CSV file extracted from Ansys Finite Element software.
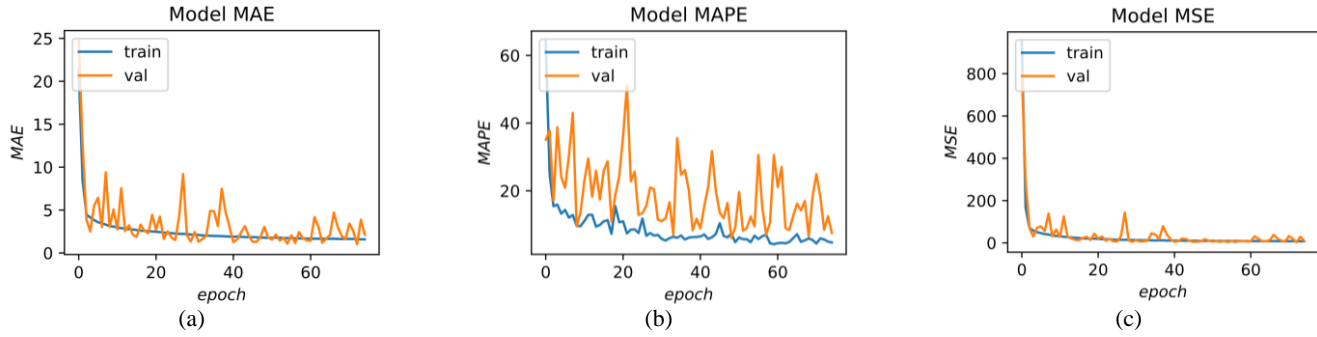

Fig.8 – Representation of metrics in function of the epochs (a) MAE; (b) MAPE; (c) MSE.

Fig.9 shows the stress fields predicted by Ansys software and by ANN, for the two cases under study: 25 and 50 mm radius. Note that the visual effect of plate deformation is neglected. Comparing the forecast obtained with the Ansys solution, the Mean Relative Error (MRE) is obtained for both situations under study, Table 2.
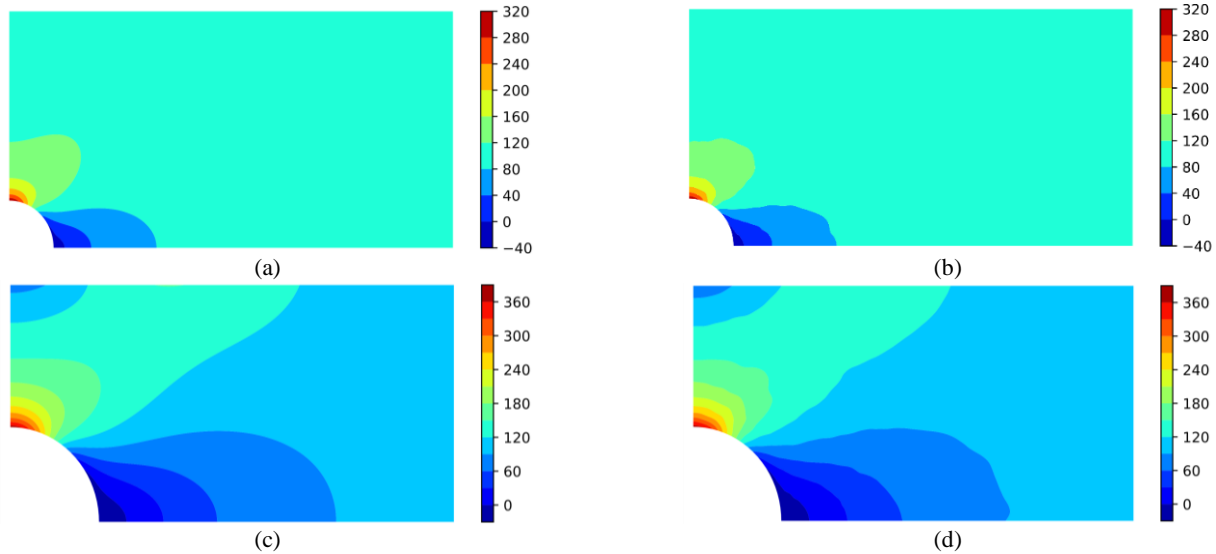
Fig.9 – Graphical comparison of the normal stress fields in the *x* direction of the plate with central hole, in MPa: (a) Ansys, *r*=25 mm; (b) ANN, *r*=25 mm; (c) Ansys, *r*=50 mm; (d) ANN, *r*=50 mm.

Moreover, the computational consumption of the two methods is analysed, namely Ansys and ANN to obtain the necessary data for the characterization of the stress field. For this, a comparison of the time spent in each of the methods to calculate the stresses is established. Note that both situations were performed with the *Intel(R) i7-4710HQ CPU @ 2.50GHz* processor and with *16 GB* of installed memory (RAM). These values are recorded in Table 2, along with the time it takes the ANN to train.

Table 2 - Results overview of the approximation and computational cost.

r (mm)	MRE (%)	Ansys (s)	ANN (s)	Training (min)
25	2.54	3	0.05	
50	6.59	3	0.03	3.24

6. Discussion and Conclusion

As can be seen in Fig.9, the stress maps are very similar, both in terms of the stress values and their distribution over the plate. The major differences lie in the limits between different contour regions of the stress maps, where there is a greater irregularity in the map predicted by the ANN. Also, from Table 2 results it is substantiated that the error is acceptable for both situations, with a MRE of 2.54% for the 25 mm radius and 6.59% for the 50 mm radius.

At the temporal level, compared to Ansys, the ANN is 59 times faster at determining the stress field for *r* equal to 25 mm and almost 100 times faster for *r* equal to 50 mm. For the case under analysis, it takes about 3.24 minutes to train the network. Despite being a high value, when compared to the simulation time, it only must be done once. After the network is trained, it is possible to predict any type of input data very quickly, when compared to a traditional finite element calculation.

Thus, it is concluded that this first ANN implementation is able to correctly and effectively predict the normal stress for a given radius value and for any point on the plate, keeping the remaining properties constant. In this way, computational costs can be significantly reduced, since the ANN can calculate, on average, the stress field 79 times faster than a classical finite element software. The forecast error is considered acceptable, presenting an MRE of 4.57% based on the two cases, where the greatest differences reside within the region's boundaries. The main disadvantages of ANN are the database building process to train the network, and the required time for training. Regarding the database, to improve the process, a script based on APDL command language is adopted. The needed time to train the network could represent a significant computational cost, but it is only necessary to perform the training once.

In conclusion, this work made it possible to highlight the potentialities of ANN in applied to stress/strain calculation in solid mechanics: shorter response time, less computational resources, and problem simplification, in detriment of a lower resolution/accuracy of structural behaviour. Considering these advantages, it is believed that these methods will have a significant potential impact in several applications, particularly in mechanical design. This research work is a first attempt to this topic, and it is recognized that there are many other techniques that could allow the results improvement in a more effective way.

References

[1] Goodfellow I, Bengio Y, Courviele A. Deep Learning (pp. 168-227). The MIT Press; 2016.

[2] Chollet F. Deep Learning with Python (pp. 46-52, 58-60). Manning Publications Co; 2018.

[3] Basheer IA, Hajmeer M. Artificial neural networks: fundamentals, computing, design, and application. Journal of Microbiological Methods. 2000; 43(1):3-31.

[4] Nair V, Hinton G. Rectified linear units improve restricted Boltzmann machines. In ICML'2010; 2010.

[5] Rumelhart DE, Hinton GE, Williams RJ. Learning representations by back-propagating errors. Nature. 1986; 323(6088), 533-536.

[6] Pilkey WD, Pilkey DF. Peterson's stress Concentration Factors. John Wiley & Sons Inc; 2008.

[7] Timoshenko S, Goodier JN. Theory of Elasticity. McGraw-Hill; 1951.

[8] Ribeiro J, Tavares S, Parente M. Stress–strain evaluation of structural parts using artificial neural networks. Proceedings of the Institution of Mechanical Engineers, Part L: Journal of Materials: Design and Applications; 2021.

[9] Oishi A., Yagawa G. Computational mechanics enhanced by deep learning. Computer Methods in Applied Mechanics and Engineering; 2017.

Free vibration analysis of erythrocytes using the constant strain finite elements: a 3D study

M. I. A. Barbosa [1], J. Belinha [2], R. Natal Jorge [3]

[1]*inesbarbosa.ma@gmail.com; INEGI, Rua Dr. Roberto Frias, 400, 4200-465; Porto; Portugal*
[2] *job@isep.ipp.pt; ISEP, Rua Dr. António Bernardino de Almeida, 431, 4249-015; Porto; Portugal*
[3] *rnatal@fe.up.pt; FEUP, Rua Dr. Roberto Frias, 4200-465 Porto, Portugal*

Abstract

Red blood cells (RBCs), also called erythrocytes, represent an important component of blood and are responsible for one of its main functions, the transport of oxygen to the entire body, which is essential for human life. As other cells of the human body, associated with a specific pathology, RBCs can present their properties and features changed in a singular way. For instance, changes in the cell geometry lead to a distinct mechanical response. Usually, each body possesses a specific natural vibration frequency, which is associated with its geometry, stiffness and mass. This characteristic allows to develop new treatments and forms of diagnosis by targeting pathologic cells possessing a natural vibration frequency different from the healthy ones. Thus, the objective of this work is to analyse the behaviour of RBCs, both normal and with well-known pathologies, using the finite element method (FEM). For this, 3D models were constructed and free vibration simulations were performed. The first four vibration modes of the different types of RBCs were qualitatively analysed. Potential fields were constructed based on the vibration modes obtained with the FEM analysis, such as potential displacement field and stress potential fields. The simulation was performed resorting to constant strain finite elements. In the end, as expected, it was possible to conclude that alterations in the initial geometry of RBCs imply significant changes in the cell mechanical response.

1. Introduction

RBCs present a simple biological structure, without nucleus or cellular organelles, and their cytoplasm is made up of 95% haemoglobin. Due to this last property, RBCs are responsible for taking oxygen to and from the tissues, which is one of the most important functions in the human body [1]. Their mechanical properties, integrity, and biological functions are dependent on the cellular membrane and their elastic protein network is responsible for their shear elastic properties [2, 3].

As other cells, RBCs can present changes in their mechanical properties, specially, in their deformability, due to some pathologies. Some examples of pathologies that affect RBCs are sickle cell anaemia, spherocytosis, or malaria. All of these represent a major problem and challenge for the medical field since they are associated with a large number of deaths, every year [4, 5]. In order to overcome these problems, several attempts have been made to understand the behaviour of normal and pathological RBCs. In the computational biomechanics field, several numerical simulations have been made and, currently, they are considered as a powerful tool to perform different types of analyses [6, 7].

Regarding the natural vibration frequency, due to its geometry and material properties, all bodies possess unique vibration frequencies and vibration modes. Such structural signature can be modified if the structure changes its geometry or its stiffness or its mass [8]. For instance, under some pathologies, RBCs modify their geometry and, therefore, change their vibration response. It is expected to capture such changes resorting to biomechanical simulations. Note that, this modification in the natural frequency of vibration of RBCs has not yet been completely understood.

In the biomechanical simulations field, several methods are currently used to analyse RBCs. From these, it is possible to highlight the Finite Element Method (FEM) [9, 10] or the Dissipative Particle Dynamics (DPD) method [11, 12]. Also, 2D models are usually used to perform the analyses, since they are simple, present low computation costs, and are often sufficient to obtain a suitable approximation. Regarding research works using this type of models, some examples are

presented in [13] and [14]. However, it is important to stress that RBCs are 3D structures so, to obtain more realistic analyses, 3D models should be considered, and some examples are already presented in [15] and [16].

Thus, the objective of the present work is to qualitatively analyse normal and pathological RBCs models, in terms of natural vibration frequency, and potential von Mises effective stress profiles. For such purpose, three distinct forms of RBCs were created (one healthy normal RBCs and two abnormal RBCs related to ovalocytosis and sickle cell anaemia), and analysed in FEMAS® (Finite Element and Meshless Analysis Software), a freeware academic software (cmech.webs.com), using 3D constant strain finite elements.

2. Finite Element Method

Emerged in the 1950's, the FEM is the most popular mesh-dependent method. However, it was only used in biomechanics for the first time in 1972 [17, 18]. This method is currently a powerful numerical tool that allows the resolution of a large and complex system of equations, being an effective tool to modulate systems in a wide range of fields [17, 19]. As other discretization techniques, the domain is divided in partitions, and each partition is linked to the other partitions of the domain by shared borders, which allows the formation of a mesh [20]. In the case of the FEM, the domain is discretized in finite elements that are connected by nodes, with a pre-establish configuration, which allows to form a mesh [21]. From these elements, linear functions, known as shape functions, are constructed and the approximated distribution of the variable under study is obtained, in order to establish the equations that allow to find the global system of equations [18]. By solving the global system of equations, the field variables are obtained, acquiring an approximate solution [21, 22]. Note that, the number of nodes and elements, the geometry of the problem, the mesh configuration and boundary conditions affect the computational time of the analysis and the accuracy of the obtained results [22]. Regarding the advantages of the FEM, it presents a simple discretization concept, a low computational cost, and results possessing a satisfactory degree of accuracy. Furthermore, FEM is easy to program and allows to analyse irregular surfaces easily. Besides this, it is possible to combine different materials and boundary conditions in the same body [17, 23]. However, in large deformation problems, the distortion of the mesh decreases the accuracy and the stability of the results [17].

3. Discrete system of equations

If a structure is exposed to loads/forces, it becomes stressed and, thus, strained, which can be understood as deformations or relative displacements. However, to analyse a deformation, alterations in the configuration of the body should be considered and this is usually expressed in terms of stress and strain, which allows to define the virtual work as the integral over the body volume [24]. Thus, the stress tensor can be defined as:

$$\boldsymbol{\sigma} = \left\{ \sigma_{xx} \quad \sigma_{yy} \quad \sigma_{xy} \right\}^T \tag{1}$$

and the strain tensor as:

$$\boldsymbol{\varepsilon} = \left\{ \varepsilon_{xx} \quad \varepsilon_{yy} \quad \varepsilon_{xy} \right\}^T \tag{2}$$

Regarding these two variables, it is possible to define them as: $\boldsymbol{\varepsilon} = \boldsymbol{Lu}$ and $\boldsymbol{\sigma} = \boldsymbol{c\varepsilon}$, with $\boldsymbol{c}$ as the material constitutive matrix. Resorting to the Galerkin weak form, it is possible to obtain the discrete equation system. With this, the solution that allows to obtain the more accurate configuration, in terms of displacements, is the one that minimizes the Lagrangian functional (L), which is defined as:

$$L = T - U + W_f \tag{3}$$

where T represents the kinetic energy, U the strain energy and W_f the work performed by the external forces, which can be defined, respectively, as:

$$T = \frac{1}{2} \int_\Omega \rho\, \dot{\mathbf{u}}^T \dot{\mathbf{u}}\, d\Omega$$

$$U = \frac{1}{2} \int_\Omega \boldsymbol{\varepsilon}^T \boldsymbol{\sigma} d\Omega \tag{4}$$

$$W_f = \int_\Omega \boldsymbol{u}^T \boldsymbol{b} \, d\Omega + \int_{\Gamma_t} \boldsymbol{u}^T \boldsymbol{t} \, d\Gamma_t$$

Note that, $\dot{\boldsymbol{u}}$ is the velocity, and ρ the density of the solid. If the functional is integrated with respect to time and then minimized, following the principle of virtual work and assuming the relations $\boldsymbol{\sigma} = \boldsymbol{c}\boldsymbol{\varepsilon}$ and $\boldsymbol{\varepsilon} = \boldsymbol{Lu}$, four equation terms will be obtained [24]:

$$\delta \boldsymbol{u_S}^T \underbrace{\int_\Omega \boldsymbol{H}_I^T \boldsymbol{\rho} \, \boldsymbol{H}_I \, d\Omega}_{\boldsymbol{M}} \ddot{\boldsymbol{u}} + \delta \boldsymbol{u_S}^T \underbrace{\int_\Omega \boldsymbol{B}_I^T \, \boldsymbol{c} \, \boldsymbol{B}_I \, d\Omega}_{\boldsymbol{K}} \boldsymbol{u} - \delta \boldsymbol{u_S}^T \underbrace{\int_\Omega \boldsymbol{H}_I^T \boldsymbol{b} \, d\Omega}_{\boldsymbol{f}_b} - \delta \boldsymbol{u_S}^T \underbrace{\int_{\Gamma_t} \boldsymbol{H}_I^T \, \bar{\boldsymbol{t}} \, d\Gamma_t}_{\boldsymbol{f}_t} = 0 \tag{5}$$

with $\boldsymbol{B}_I$ as the deformability matrix, $\boldsymbol{H}_I$ is the diagonal matrix containing the shape functions, $\boldsymbol{b}$ is the body force vector actuating in the solid domain Ω and $\bar{\boldsymbol{t}}$ is the traction force vector actuating in the domain boundary Γ_t.

In the end, the equilibrium equation is found and defined as:

$$\boldsymbol{M}\ddot{\boldsymbol{u}} + \boldsymbol{K}\boldsymbol{u} = \boldsymbol{F} \tag{6}$$

where $\boldsymbol{K}$ represents the stiffness matrix, $\boldsymbol{M}$ is the mass matrix, $\ddot{\boldsymbol{u}}$ and $\boldsymbol{u}$ are the acceleration and displacement field, respectively, and $\boldsymbol{F}$ the vector of forces that include both the body weight vector ($\boldsymbol{f}_b$) and the external forces vector ($\boldsymbol{f}_t$). Following the demonstration shown in [24], in order to obtain the vibration modes and vibration frequencies, it is necessary to neglect the applied forces, $\boldsymbol{F}$, and solve the following equation,

$$\det\!\left(\boldsymbol{K} - \omega^2 \boldsymbol{M}\right) \boldsymbol{\Phi} = \boldsymbol{0} \tag{7}$$

The solution will provide $3N$ vibration frequencies ω, being N the number of nodes discretizing the problem domain, and $3N$ vectors $\boldsymbol{\Phi}$ with size $[3N \times 1]$ representing the vibration modes. The first vibration mode, corresponding to the lowest energy mode, is known as natural frequency and its corresponding vibration mode is its natural vibration mode. The vibration frequencies and their corresponding vibration modes are the Eigen-values and Eigen-vectors of equation (2).

4. Numerical Results

For the present work, three different 3D geometries of RBCs were created, one presenting a normal healthy RBC (H), and the other two representing a RBC affected by sickle cell anaemia (SCA) and ovalocytosis (also known as hereditary elliptocytosis) (O). Note that, all models were created following realistic geometries (an average diameter of $7.5\mu m$), based on data presented in the literature [25] and a representation of each one is presented next. Moreover, the mechanical properties (Young's modulus and Poisson's coefficient [25]) used for each model are presented in Table 1. All the cells possess the same density: $1.110 \times 10^{-9} kg/\mu m^3$.

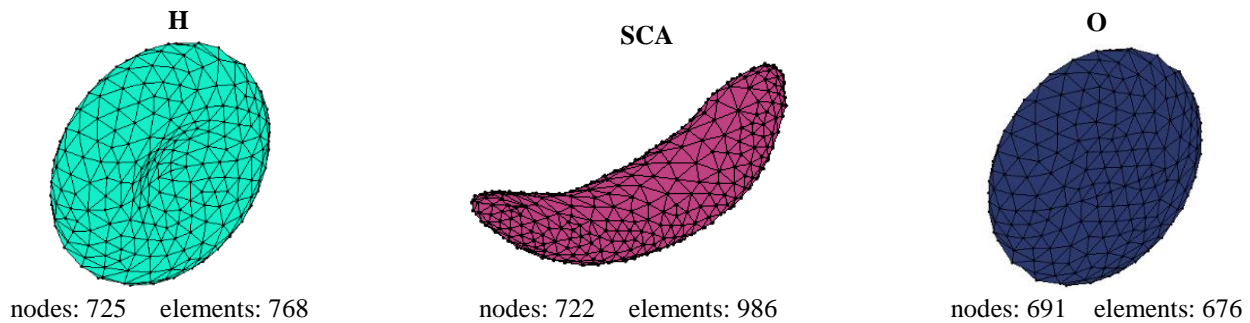| H	SCA	O
nodes: 725 elements: 768	nodes: 722 elements: 986	nodes: 691 elements: 676

Fig.4 –The three models used, where H represents the healthy RBC, SC a cell affected by sickle cell anaemia and O by ovalocytosis.

Table 1 –Values of Young's modulus and Poisson coefficient for the three different cases [25].
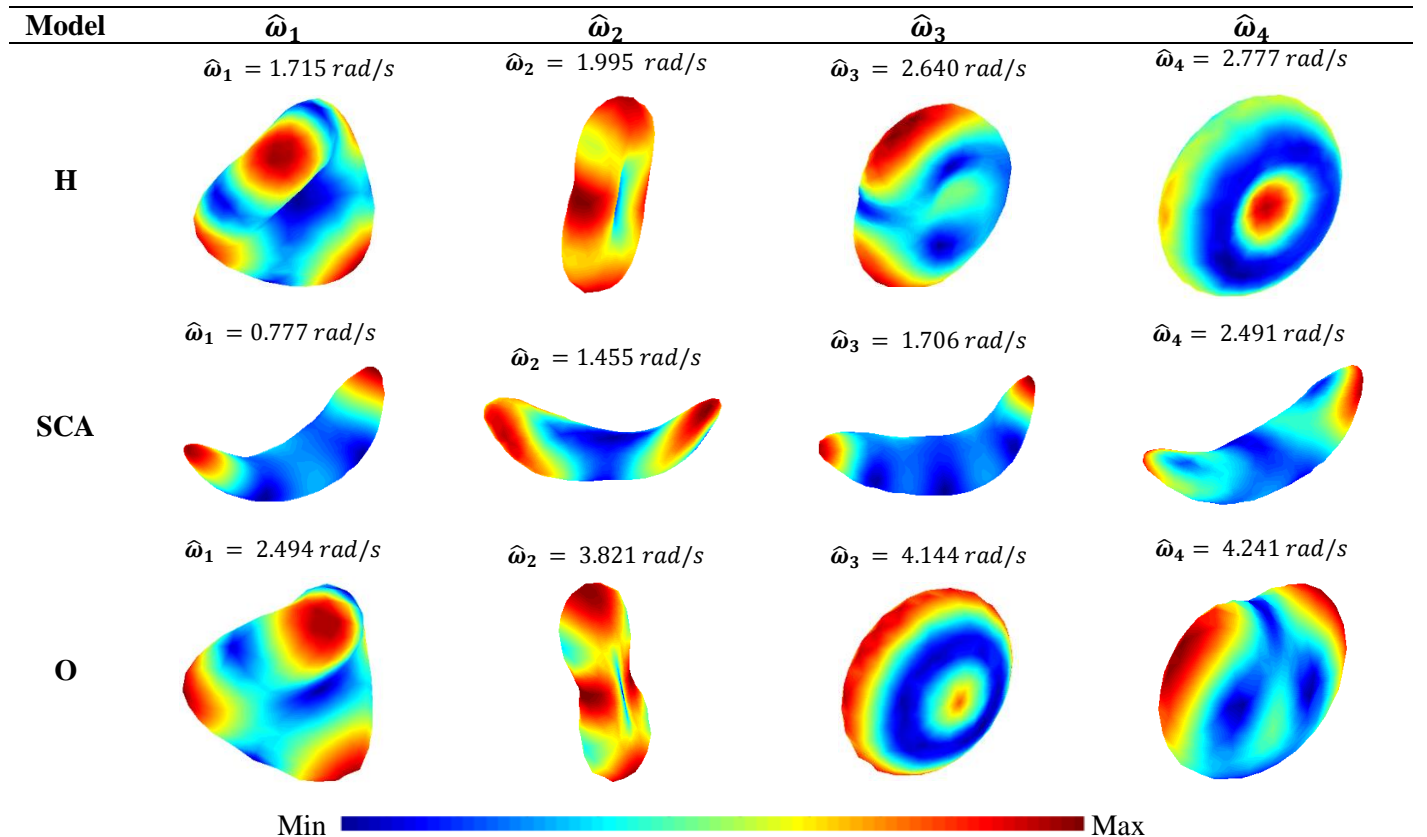
RBC	Young's Modulus (N/µm^2)	Poisson's Coefficient
H	2,6×10^{-8}	0,499
SCA	3,7143×10^{-8}	0,45
O	8,423×10^{-8}	0,45

The analyses of the first four modes of vibration were performed in FEMAS®, for each case, and it was imposed that cells can vibrate freely, i.e., no degree of freedom was constrained. The results obtained are presented in Tables 2 and 3.

Analysing the results presented in Table 2, it is possible to visualise that different geometries of RBCs led to different values of vibration frequency, as expected. Besides that, it is also possible to visualise that each vibration frequency is associated with a vibration mode (deformed shape of the RBCs). Such vibration mode corresponds to the potential deformation that the RBC will experience when excited with the corresponding vibration frequency. Thus, low vibration frequencies (low energy frequencies) induce simpler vibration modes, and higher vibration frequencies correspond to more complex vibration modes shapes. In the results, it is also possible to note that the final vibration modes shapes of the H and O models are similar since the initial models also present comparable geometries. However, since they are not equal, the vibration frequencies are different, as expected.

Notice that the models can vibrate by resonance if a vibration frequency is externally induced (an ultra-sound source, for instance). Thus, the lowest vibration frequency is always the first to be identified by resonance, corresponding to the lowest energy vibration frequency (this first vibration frequency is known as natural frequency). As expected, the results show that low energy vibration frequencies are associated with simple vibration modes and as the model's vibration frequency increases, the vibration mode becomes more complex. This observation is valid for all presented figures.

Despite the model under analysis (H, SCA or O), notice that the results show that the first vibration frequency is always very different from the other vibration frequencies. This allows to clearly identify the natural vibration mode, by a comfortable large margin, allowing to suggest a value for potential therapies or diagnostics.

Table 2 - Colour map of the first four free vibration modes and corresponding vibration frequencies ($\widehat{\omega}_{1,2,3\ and\ 4}$) obtained with FEM.

Model	$\widehat{\omega}_1$	$\widehat{\omega}_2$	$\widehat{\omega}_3$	$\widehat{\omega}_4$
H	$\widehat{\omega}_1 = 1.715\ rad/s$	$\widehat{\omega}_2 = 1.995\ rad/s$	$\widehat{\omega}_3 = 2.640\ rad/s$	$\widehat{\omega}_4 = 2.777\ rad/s$
SCA	$\widehat{\omega}_1 = 0.777\ rad/s$	$\widehat{\omega}_2 = 1.455\ rad/s$	$\widehat{\omega}_3 = 1.706\ rad/s$	$\widehat{\omega}_4 = 2.491\ rad/s$
O	$\widehat{\omega}_1 = 2.494\ rad/s$	$\widehat{\omega}_2 = 3.821\ rad/s$	$\widehat{\omega}_3 = 4.144\ rad/s$	$\widehat{\omega}_4 = 4.241\ rad/s$

Min ████████████████ Max

Assuming the ith vibration mode as potential displacement fields, $\bar{\boldsymbol{u}}_i = \boldsymbol{\Phi}_i$, it is possible to obtain the corresponding stress field, $\bar{\boldsymbol{\sigma}}_i = \boldsymbol{c}\bar{\boldsymbol{\varepsilon}}_i$. With this field, it is possible to establish the von Mises effective stress field, $\bar{\bar{\sigma}}_i$,

$$\bar{\bar{\sigma}}_i = \sqrt{\frac{3}{2}\left(\bar{\boldsymbol{\sigma}}_i - \frac{1}{3}tr(\bar{\boldsymbol{\sigma}}_i)\boldsymbol{I}\right):\left(\bar{\boldsymbol{\sigma}}_i - \frac{1}{3}tr(\bar{\boldsymbol{\sigma}}_i)\boldsymbol{I}\right)} \tag{8}$$

The results shown in Table 3 are only qualitative results. The magnitude $\bar{\bar{\sigma}}_i$ is not relevant, because it was obtained for a potential (fictitious) displacement field, $\bar{\boldsymbol{u}}_i$. Nevertheless, it is possible to visualize and analyse the locations in which higher levels of the von Mises effective stress field, $\bar{\bar{\sigma}}_i$, will occur in the RBCs. Therefore, the distributions shown in Table 3 represent this field. For the H-RBCs, the first vibration mode induces higher stress values near the border of the RBC. In contrast, for the SCA-RBCs and the O-RBC, the corresponding first vibration mode leads to higher stress values in the centre of the RBC. Concerning the O-RBC, this result was not expected. Observing Table 2, the first vibration modes of the H-RBCs and O-RBC are very similar. Thus, expectedly these two cells should present a similar stress field. Such results indicate that sub-surface deformations are occurring inside the RBC that influence significantly the final stress fields. These results are relevant since they provide the locations of the RBC in which the stress field shows higher values in a resonance scenario, indicating the potential rupture sites of the RBC.

Table 3 - Colour map of the von Mises effective stress fields $\bar{\bar{\sigma}}_i$ of the first four free vibration modes ($\hat{\omega}_{1,2,3\ and\ 4}$) obtained with FEM.

Model	$\hat{\omega}_1$	$\hat{\omega}_2$	$\hat{\omega}_3$	$\hat{\omega}_4$
H				
SCA				
O				

Min ◼ Max
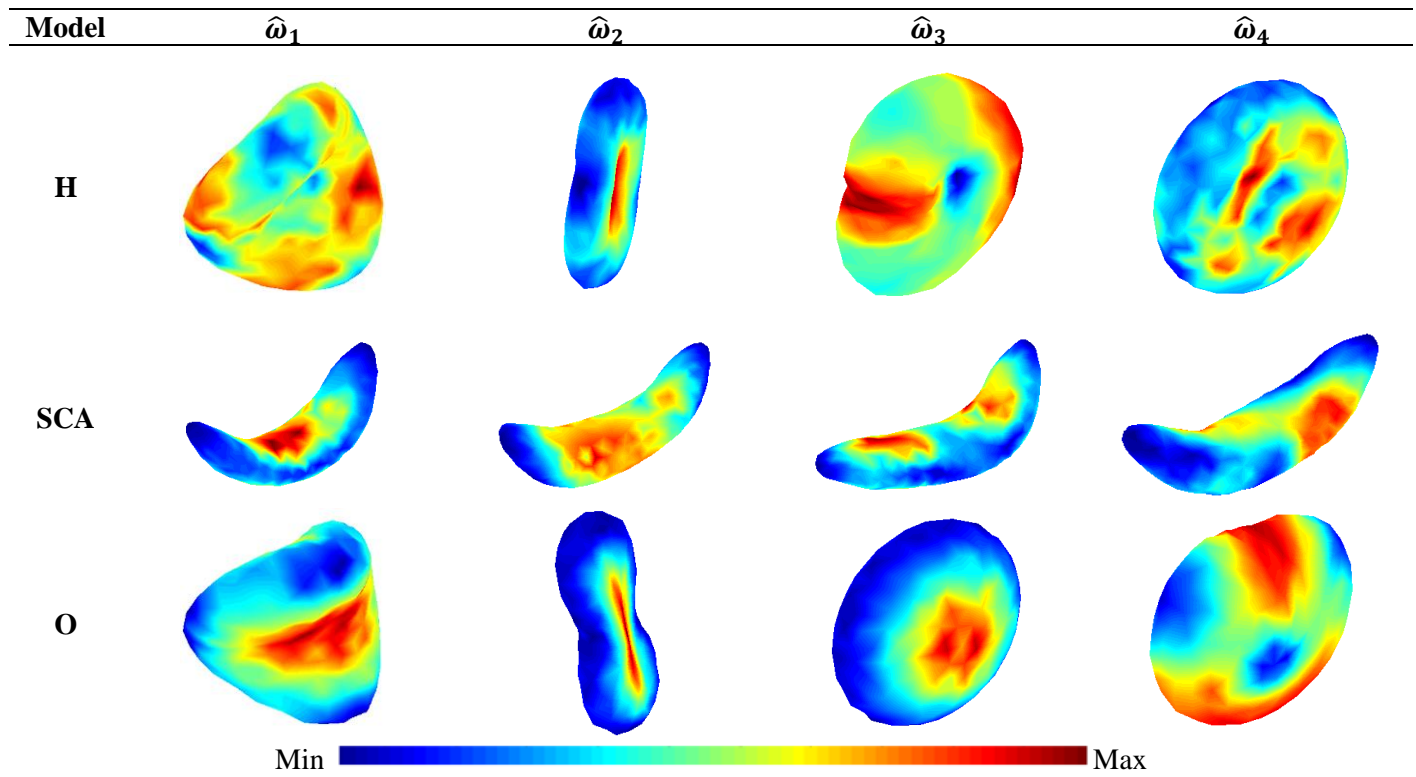
5. Conclusion

Diseases related to RBCs affect a large number of people, representing a severe impact on the quality of life of the patients and also on the economy, due to the high cost associated to them. As in other cells, different pathologies can influence the natural structure and the properties of the RBCs in different ways. This way, the use of numerical simulations can be useful to understand and overcome diseases related to these cells. Thus, the objective of the present work was to qualitatively analyse the first four modes of vibration of the RBCs. For this, a constant strain 3D FEM was

used and three 3D models (one representing a normal RBC, and another two representing two specific diseases related to RBC, the sickle cell anaemia and ovalocytosis) were constructed and analysed.

Regarding the natural frequencies obtained for each geometry, this study allows to predict the following natural frequencies for each RBC: $\widehat{\omega}_1^H = 1.715 \, rad/s$, $\widehat{\omega}_1^{SCA} = 0.777 \, rad/s$ and $\widehat{\omega}_1^0 = 2.494 \, rad/s$. As it is possible to verify, each kind of geometry possesses a unique and very distinct natural frequency. Thus, in the future, using this knowledge, it will be possible to design diagnosis procedures capable to identify the fraction of pathological RBCs per volume using ultrasonic techniques. More, if the aim is to eliminate pathologic RBCs, the ultrasonic technique can be used to excite blood volumes with the same frequency as the natural frequency of the pathological RBC and induce resonance. The resonance will lead to the collapse of the pathologic RBC following the red areas represented in Table 3, leaving the healthy RBCs and other cell and structures unharmed. This technique is already used in kidney stone treatment by shock wave (high-energy sound waves).

This study presents some limitations, as for instance, the low number of nodes used in the discretization, which might influence the accuracy of the final results, and the lack of involving material (fluid). This way, in the future, these parameters should be improved, and convergence tests must be done to obtain the ideal values for each model.

Acknowledgements and Funding

References

[1]   Buys, A.V., et al., Changes in red blood cell membrane structure in type 2 diabetes: a scanning electron and atomic force microscopy study. Cardiovascular diabetology, 2013. 12(1): p. 25.

[2]   Chasis, J.A. and S.B. Shohet, Red cell biochemical anatomy and membrane properties. Annual review of physiology, 1987. 49(1): p. 237-248.

[3]   Elgsaeter, A. and A. Mikkelsen, Shapes and shape changes in vitro in normal red blood cells. Biochimica et Biophysica Acta (BBA)-Reviews on Biomembranes, 1991. 1071(3): p. 273-290.

[4]   Suresh, S., Mechanical response of human red blood cells in health and disease: Some structure-property-function relationships. Journal of materials research, 2006. 21(8): p. 1871-1877.

[5]   Pereira, M., et al., Trends in prevalence of diabetes mellitus and mean fasting glucose in Portugal (1987–2009): a systematic review. Public Health, 2014. 128(3): p. 214-221.

[6]   Bodnár, T. and A. Sequeira, Numerical simulation of the coagulation dynamics of blood. Computational and Mathematical Methods in Medicine, 2008. 9(2): p. 83-104.

[7]   Ataullakhanov, F.I. and M.A. Panteleev, Mathematical modeling and computer simulation in blood coagulation. Pathophysiology of haemostasis and thrombosis, 2005. 34(2-3): p. 60-70.

[8]   Monteiro, M.O., et al., Effect on osmotic fragility of red blood cells of whole blood submitted to vibrations in an oscillating platform. African Journal of Biotechnology, 2011. 10(64): p. 14197-14202.

[9]   Dao, M., C.T. Lim, and S. Suresh, Mechanics of the human red blood cell deformed by optical tweezers. Journal of the Mechanics and Physics of Solids, 2003. 51(11-12): p. 2259-2280.

[10] Liu, W.K., et al., Immersed finite element method and its applications to biological systems. Computer methods in applied mechanics and engineering, 2006. 195(13-16): p. 1722-1749.

[11] Fedosov, D.A., H. Noguchi, and G. Gompper, Multiscale modeling of blood flow: from single cells to blood rheology. Biomechanics and modeling in mechanobiology, 2014. 13(2): p. 239-258.

[12] Peng, Z., et al., Lipid bilayer and cytoskeletal interactions in a red blood cell. Proceedings of the National Academy of Sciences, 2013. 110(33): p. 13356-13361.

[13] Hosseini, S.M. and J.J. Feng, A particle-based model for the transport of erythrocytes in capillaries. Chemical engineering science, 2009. 64(22): p. 4488-4497.

[14] Polwaththe-Gallage, H.-N., S.C. Saha, and Y. Gu, Deformation properties of single red blood cell in a stenosed microchannel. 2013

[15] Hosseini, S.M. and J.J. Feng, How malaria parasites reduce the deformability of infected red blood cells. Biophysical journal, 2012. 103(1): p. 1-10.

[16] Wu, T. and J.J. Feng, Simulation of malaria-infected red blood cells in microfluidic channels: Passage and blockage. Biomicrofluidics, 2013. 7(4): p. 044115.

[17] Belinha, J., et al., The analysis of laminated plates using distinct advanced discretization meshless techniques. Composite Structures, 2016. 143: p. 165-179.

[18] Geng, J.-P., K.B. Tan, and G.-R. Liu, Application of finite element analysis in implant dentistry: a review of the literature. The Journal of prosthetic dentistry, 2001. 85(6): p. 585-598.

[19] Belinha, J., et al., The natural neighbor radial point interpolation method extended to the crack growth simulation. International Journal of Applied Mechanics, 2016. 8(01): p. 1650006.

[20] Peyroteo, M., et al., Mechanical bone remodelling: Comparative study of distinct numerical approaches. Engineering Analysis with Boundary Elements, 2018.

[21] Belinha, J., Meshless Methods: The Future of Computational Biomechanical Simulation. J Biom Biostat 2016. 7: p. 325.

[22] Chandran, K.B., S.E. Rittgers, and A.P. Yoganathan, Biofluid mechanics: the human circulation. 2006: CRC press.

[23] Parashar, S.K. and J.K. Sharma, A review on application of finite element modelling in bone biomechanics. Perspectives in Science, 2016. 8: p. 696-698.

[24] Belinha, J., Meshless methods in biomechanics. Bone tissue remodelling analysis, 2014.

[25] Tomaiuolo, G., *Biomechanical properties of red blood cells in health and disease towards microfluidics.* Biomicrofluidics, 2014. 8(5): p. 051501.